

1     **(a) The point-by-point response to the reviews**

2     Dear Referee #2,

3     We thank you for your review of our manuscript and your detailed  
4     remarks. We would like to improve the article here in an immediate reply.

5     Please, find our answers/comments on your notes below:

6     (1) p. 5, l. 108: ...from the thousands of channels' observations... please  
7     rephrase, but I have no suggestions

8     Yes, you are right.

9     “It is important to properly ... from the thousands of channels’  
10    observations ....” has been modified to “In order to improve the  
11    calculation efficiency and retrieval quality, it is very important to properly  
12    select a set of channels that can provide as much information as possible.”  
13    (L 104-L 107)

14    Thanks.

15    (2) p. 8, l. 155: Channel selection mostly uses the information content  
16    and delivers the largest amount of information for the selected channel  
17    combination during the retrieval.

18    Yes, you are right.

19    “Currently, information content is often employed in channel selection.  
20    During retrieval, this method delivers the largest amount of information  
21    for the selected channel combination (Rodgers, 1996; Du et al., 2008; He  
22    et al., 2012; Richardson et al., 2018).” has been modified to “Channel

23 selection mostly uses the information content and delivers the largest  
24 amount of information for the selected channel combination during the  
25 retrieval (Rodgers, 1996; Du et al., 2008; He et al., 2012; Richardson et  
26 al., 2018).” (L 153-L 156)

27 Thanks.

28 (3) p. 9, l. 194: after the retrieval

29 Yes, you are right.

30 “...after retrieval” has been modified to “...after the retrieval” (L 193)

31 Thanks.

32 (4) p. 11, l. 236: (2) The number looks like an equation number, so it is a  
33 bit confusing.

34 Sorry for the confusion.

35 The step number has been modified to (I), (II), (III) and (IV). (L 222; L  
36 234; L 255; L 270; L 272)

37 Thanks.

38 (5) p. 18, l. 389: The footprint size is 13.5 km

39 Yes, you are right.

40 This has been modified. (L 288)

41 Thanks.

42 (6) p. 19, l. 401/402: in Fig. 1. The measurement error is not below 0.2K  
43 for all the instrument channels. There are...

44 Yes, you are right.

45 “The root mean square error of an AIRS infrared channel is shown in Fig.  
46 1, with black spots, indicating that not all the instrument channels possess  
47 a measurement error of less than 0.2 K.” has been modified to “The root  
48 mean square error of an AIRS infrared channel is shown in Fig. 1. The  
49 measurement error is not below 0.2K for all the instrument channels.” (L  
50 400-L 401)

51 Thanks.

52 (7) p. 21, l. 434: ranking -> in the range

53 Yes, you are right.

54 This has been modified. (L 432)

55 Thanks.

56 (8) p. 27, l. 532: temperature, a better observation can be obtained for  
57 higher temperatures

58 Yes, you are right.

59 “...temperature, the higher temperature is, the better observation can be  
60 obtained;” has been modified to “...temperature, a better observation can  
61 be obtained for higher temperatures” (L 524-L 525)

62 Thanks.

63 (9) p. 28, l. 547: to the -> at

64 Yes, you are right.

65 This has been modified. (L 538)

66 Thanks.

67 (10) p. 30, l. 567: reach to -> reaches

68 Yes, you are right.

69 This has been modified. (L 560)

70 Thanks.

71 (11) p. 36, l. 650: humidity and 10m wind speed (remove dot after speed)

72 Sorry for my carelessness.

73 This has been modified. (L 643)

74 Thanks.

75 (12) p. 43, l. 778: to the -> at

76 Yes, you are right.

77 This has been modified. (L 771; L 828)

78 Thanks again for your careful review.

79

80 Dear Referee #4,

81 We thank you for your review of our manuscript and your detailed

82 remarks. We would like to improve the article here in an immediate reply.

83 Please, find our answers/comments on your notes below:

84 (1) p1, l16-20: Suggest to replace the first two sentences of the abstract

85 by: "This study introduces an effective channel selection method for

86 hyperspectral infrared sounders. The method is illustrated for the

87 Atmospheric InfraRed Sounder (AIRS) instrument."

88 Yes, we agree with you.

89 This has been modified. (L 16-L 18)

90 Thanks.

91 (2) p1, l21: "improved method" -> "improved channel selection (ICS)

92 method"

93 Yes, you are right.

94 This has been modified. (L 19-L 21)

95 Thanks.

96 (3) p2, l24: suggest to delete "and closer to the actual atmosphere"

97 Yes, you are right.

98 This has been deleted. (L 22)

99 Thanks.

100 (4) p2, l30: suggest to replace "In general, ..." by "Also at lower

101 heights, ..."

102 Yes, you are right.

103 This has been modified. (L 28)

104 Thanks.

105 (5) p2, l31-32: delete "(Improved Channel Selection)"

106 Yes, you are right.

107 This has been deleted. (L 29)

108 Thanks.

109 (6) p2, l32-36: suggest to rephrase this as "Statistical inversion

110 comparison experiments for four different regions illustrate latitudinal

111 and seasonal variations and better performance of ICS compared to the  
112 NWP Channel Selection (NCS) and Primary Channel Selection (PCS)  
113 methods. The ICS method shows potential for future applications."

114 Yes, we agree with you.

115 "Statistical inversion comparison experiments in four typical regions  
116 indicate that ICS in this paper is significantly better than NCS (NWP  
117 Channel Selection) and PCS (Primary Channel Selection) in different  
118 regions and shows latitudinal variations, which shows potential for future  
119 applications." has been modified to "Statistical inversion comparison  
120 experiments for four different regions illustrate latitudinal and seasonal  
121 variations and better performance of ICS compared to the NWP Channel  
122 Selection (NCS) and Primary Channel Selection (PCS) methods. The ICS  
123 method shows potential for future applications." (L 30-L 34)

124 Thanks.

125 (7) p4, 170: please fix: "Infrared Atmospheric Sounding Interferometer"

126 Yes, you are right.

127 This has been modified. (L 68-L 69)

128 Thanks.

129 (8) p5, 1110: replace "the channel selection algorithm" by "channel  
130 selection algorithms"

131 Yes, you are right.

132 This has been modified. (L 108)

133 Thanks.

134 (9) p11, l236: replace "p matrix" by "for calculating the p value"?

135 Yes, you are right.

136 This has been modified. (L 234)

137 Thanks.

138 (10) p11, l237: replace "matrixes, it" by "matrices, they"

139 Yes, you are right.

140 This has been modified. (L 235)

141 Thanks.

142 (11) p12, l257: replace "According to" by "Using"

143 Yes, you are right.

144 This has been modified. (L 257)

145 Thanks.

146 (12) p18, l383: The reference to Hoffmann and Alexander (200) can be

147 deleted here, I think. Maybe move reference to Susskind et al. (2003)

148 from line 389 to this place.

149 Yes, we agree with you.

150 “...(Aumann et al., 2003; Hoffmann and Alexander, 2009).” has been

151 modified to “...(Aumann et al., 2003; Susskind et al., 2003).”. (L

152 382-L383)

153 “Susskind et al. (2003)” has been deleted. (L 388)

154 Thanks.

(13) p27, 1515-534: Suggest to delete all the sentences relating the wavelengths to the wavenumbers, as this is trivial. For instance, replace "When the wavenumber approaches 1000... Near this band..." by "Near the 10  $\mu\text{m}$  band..."

Yes, you are right.

“(1) When the wavenumber approaches 1000, the wavelength is 10  $\mu\text{m}$  (1/1000  $\text{cm}^{-1}$ ). Near this band, fewer channels are selected by PCS because the retrieval of ground temperature is considered by NCS; (2) When the wavenumber is near 1200, the wavelength is 9  $\mu\text{m}$  (1/1200  $\text{cm}^{-1}$ ). Near this band, no channels are selected by PCS because the retrieval of O<sub>3</sub> is not considered in this paper; (3) When the wavenumber approaches 1500, the wavelength is 6.7  $\mu\text{m}$  (1/1500  $\text{cm}^{-1}$ ). As is known, the spectral range from 6  $\mu\text{m}$  to 7  $\mu\text{m}$  corresponds to water vapor absorption bands, but fewer channels are selected by NCS; (4) When the wavenumber is close to 2000, it derives a wavelength of 5  $\mu\text{m}$  (1/2000  $\text{cm}^{-1}$ ), which includes 4.2  $\mu\text{m}$  for N<sub>2</sub>O and 4.3  $\mu\text{m}$  for CO<sub>2</sub> absorption bands.” has been modified to “(1) Near 10  $\mu\text{m}$  band, fewer channels are selected by PCS because the retrieval of ground temperature is considered by NCS; (2) Near 9  $\mu\text{m}$  band, no channels are selected by PCS because the retrieval of O<sub>3</sub> is not considered in this paper; (3) As is known, the spectral range from 6  $\mu\text{m}$  to 7  $\mu\text{m}$  corresponds to water vapor absorption bands, but fewer channels are selected by NCS; (4) Near 5  $\mu\text{m}$  band, it



177 includes 4.2  $\mu\text{m}$  for  $\text{N}_2\text{O}$  and 4.3  $\mu\text{m}$  for  $\text{CO}_2$  absorption bands.” (L  
178 514-L 521)

179 “(5) In the near infrared area, the wavenumber exceeds 2200, deriving a  
180 wavelength of less than 4  $\mu\text{m}$  ( $1/2000\text{ cm}^{-1}$ ). A small number of channels  
181 is selected by NCS, but no channels are selected by PCS.” has been  
182 modified to “(5) Near 4  $\mu\text{m}$  band, a small number of channels is selected  
183 by NCS, but no channels are selected by PCS.” (L 526-L 527)

184 Thanks.

185 (14) p27, l529-533: It is still not clear what is meant by "high temperature  
186 zone", I think. Does this refer to temperatures at high altitudes?

187 Sorry for the confusion.

188 “high temperature zone” is not clear for readers which we want to say  
189 “under the higher temperature conditions” But it can be deleted in this  
190 sentence, because we have explained it in the following sentences.

191 “PCS is favorable for atmospheric temperature observation in the high  
192 temperature zone. Because 4.2  $\mu\text{m}$  and 4.3  $\mu\text{m}$  bands are sensitive to high  
193 temperature, a better observation can be obtained for higher temperatures;”  
194 has been modified to “PCS is favorable for atmospheric temperature  
195 observation. Because 4.2  $\mu\text{m}$  and 4.3  $\mu\text{m}$  bands are sensitive to high  
196 temperature, a better observation can be obtained for higher temperatures;”  
197 (L 522-L 525)

198 “Due to the method selected in this paper, there are more channels at 4.2

199  $\mu\text{m}$  for  $\text{N}_2\text{O}$  and  $4.3 \mu\text{m}$  for  $\text{CO}_2$  absorption bands, and the channel  
200 combination of PCS is superior to that of NCS for atmospheric  
201 temperature observation in the high temperature zone.” has been modified  
202 to “Due to the method selected in this paper, there are more channels at  
203  $4.2 \mu\text{m}$  for  $\text{N}_2\text{O}$  and  $4.3 \mu\text{m}$  for  $\text{CO}_2$  absorption bands, and the channel  
204 combination of PCS is superior to that of NCS for atmospheric  
205 temperature observation.” (L 689-L 693)

206 Thanks.

207 (15) p28, l537: replaced "used in this paper" by "considered in this study"

208 Yes, you are right.

209 This has been modified. (L 528)

210 Thanks.

211 (16) p29, Fig. 5: I would like to suggest to combine the curves of plot a)  
212 and b) into a single plot.

213 Yes, you are right.

214 Fig. 5 has been modified to “The relationship between the number of  
215 iterations and ARI. Blue line represents the result of ICS. Red dotted line  
216 stands for the result of PCS.” (L 547: Fig. 5)

217 Thanks again for your careful review.

218

219

(b) The list of all relevant changes made in the manuscript

A channel selection method for hyperspectral  
atmospheric infrared sounders based on  
layering

Shujie Chang<sup>1, 2, 3</sup>, Zheng Sheng<sup>1, 2</sup>, Huadong Du<sup>1, 2</sup>, Wei Ge<sup>1, 2</sup> and  
Wei Zhang<sup>1, 2</sup>

<sup>1</sup> College of Meteorology and Oceanography, National University of  
Defense Technology, Nanjing, China

<sup>2</sup> Collaborative Innovation Center on Forecast and Evaluation of  
Meteorological Disasters, Nanjing University of Information  
Science and Technology, Nanjing, China

<sup>3</sup> South China Sea Institute for Marine Meteorology, Guangdong  
Ocean University, Zhanjiang, China

**Correspondence:** Zheng Sheng (19994035@sina.com)

**Abstract.** ~~Because a satellite channel's ability to resolve~~  
~~hyperspectral data varies with height,~~ This study introduces an  
~~improved channel selection method is proposed based on~~  
~~information content.~~ An effective channel selection ~~scheme~~ method  
for a hyperspectral ~~atmospheric~~ infrared ~~sounder using sounders.~~  
The method is illustrated for the Atmospheric InfraRed Sounder

(AIRS ~~data based on layering is proposed.~~) instrument. The results are as follows: (1) Using the improved ~~method,~~channel selection (ICS). the atmospheric retrievable index is more stable, the value reaching 0.54. The coverage of the weighting functions is more evenly distributed over height with this method ~~and closer to the actual atmosphere;~~ (2) Statistical inversion comparison experiments show that the accuracy of the retrieval temperature, using the improved channel selection method in this paper, is consistent with that of 1Dvar channel selection. In the stratosphere and mesosphere especially, from 10 hPa to 0.02 hPa, the accuracy of the retrieval temperature of our improved channel selection method is improved by about 1 K. ~~In general~~Also at lower heights, the accuracy of the retrieval temperature of ICS (~~Improved Channel Selection~~) is improved; (3) Statistical inversion comparison experiments ~~in~~for four ~~typical regions indicate that ICS in this paper is significantly different regions illustrate latitudinal and seasonal variations and~~ better ~~than NCS (performance of ICS compared to the~~ NWP Channel Selection (NCS) and ~~PCS (Primary Channel Selection) in different regions and shows latitudinal variations, which (PCS) methods. The~~ ICS method shows potential for future applications.

## 1 Introduction

264 Since the successful launch of the first meteorological satellite,  
265 TIROS in the 1960s, satellite observation technology has developed  
266 rapidly. Meteorological satellites observe the Earth's atmosphere  
267 from space and are able to record data from regions which are  
268 otherwise difficult to observe. Satellite data greatly enrich the  
269 content and range of meteorological observations, and consequently,  
270 atmospheric exploration technology and meteorological observations  
271 have taken us to a new stage in our understanding of weather  
272 systems and related phenomena (Fang, 2014). From the perspective  
273 of vertical atmospheric observation, satellite instruments are  
274 developing rapidly. In their infancy, the traditional infrared  
275 measurement instruments for detecting atmospheric temperature and  
276 moisture profiles, such as TOVS (Smith et al., 1991) or HIRS in  
277 ATOVS (Chahine, 1972; Li et al., 2000; Liu, 2007), usually  
278 employed filter spectrometry. Even though such instruments have  
279 played an important role in improving weather prediction, it is  
280 difficult to continue to build upon improvements in terms of  
281 observation accuracy and vertical resolution due to the limitation of  
282 low spectral resolution. By using this kind of filter-based  
283 spectroscopic measurement instrument, therefore, it is difficult to  
284 meet today's needs in numerical weather prediction (Eyre et al.,  
285 1993; Prunet et al., 2010; Menzel et al., 2018). To meet this

challenge, a series of plans for the creation of high-spectral resolution atmospheric measurement instruments has been executed in the United States and in Europe in recent years: One example is the AIRS (Atmospheric InfraRed Sounder) on the Earth Observation System, “Aqua”, launched on May 4, 2002 from the United States. AIRS has 2378 spectral channels providing sensitivity from the ground to up to about 65 km of altitude (Aumann et al., 2003; Hoffmann and Alexander, 2009; Gong et al., 2011). The United States and Europe, in 2010 and in 2007, also installed the CRIS (Cross-track Infrared Sounder) and the IASI (~~Inter-Attractive~~Infrared Atmospheric Sounding Interferometer) on polar-orbiting satellites.

China also devotes great importance to the development of such advanced sounding technologies. In the early 1990s, the National Satellite Meteorological Center began to investigate the principles and techniques of hyperspectral resolution atmospheric observations. China’s development of interferometric atmospheric vertical detectors eventually led to the launch of Fengyun No. 3, on May 27, 2008, and Fengyun No. 4 on December 11, 2016, both of which were equipped with infrared atmospheric instruments. How best to use the hyperspectral resolution observation data obtained from these instruments, to obtain reliable atmospheric temperature and

humidity profiles, is an active area of study in atmospheric inversion theory.

Due to technical limitations, only a limited number of channels could at first be built into the typical satellite instruments. In this case, channel selection generally involved controlling the channel weighting function by utilizing the spectral response characteristics of the channel (such as center frequency and bandwidth). With the development of measurement technology, increasing numbers of hyperspectral detectors were carried on meteorological satellites. Due to the large number of channels and data supported by such instruments today (such as AIRS with 2378 channels and IASI with 8461 channels), it has proven extremely cumbersome to store, transmit, and process such data. Moreover, there is often a close correlation between the channels, causing an ill-posedness of the inversion, potentially compromising accuracy of the retrieval product based on hyperspectral resolution data.

However, hyperspectral detectors have many channels and provide real-time mode prediction systems with vast quantities of data, which can significantly improve prediction accuracy. But, if all the channels are used to retrieve data, the retrieval time considerably increases. Even more problematic are the glut of information produced, and the unsuitability of the calculations for real-time

forecasting. Concurrently, the computer processing power must be large enough to meet the demands of simulating all the channels simultaneously within the forecast time. ~~In order to improve the calculation efficiency and retrieval quality, it is very important to properly select a groupset of channels that can provide as much information as possible from the thousands of channels' observations to improve the calculation efficiency and retrieval quality.~~

Many researchers have studied ~~the~~ channel selection ~~algorithm-algorithms~~. Menke (1984) first chose channels using a data precision matrix method. Aires et al. (1999) made the selection using the Jacobian matrix, which has been widely used since then (Aires et al., 2002; Rabier et al., 2010). Rodgers (2000) indicated that there are two useful quantities in measuring the information provided by the observation data: Shannon information content and degrees of freedom. The concept of information capacity then became widely used in satellite channel selection. In 2007, Xu (2007) compared the Shannon information content with the relative entropy, analyzing the information loss and information redundancy. In 2008, Du et al. (2008) introduced the concept of the atmospheric retrievable index (ARI) as a criterion for channel selection, and in 2010, Wakita et al. (2010) produced a scheme for calculating the information content of the various atmospheric parameters in remote sensing using



Bayesian estimation theory. Kuai et al. (2010) analyzed both the Shannon information content and degrees of freedom in channel selection when retrieving CO<sub>2</sub> concentrations using thermal infrared remote sensing and indicated that 40 channels could contain 75% of the information from the total channels. Cyril et al. (2003) proposed the optimal sensitivity profile method based on the sensitivity of different atmospheric components. Lupu et al. (2012) used degrees of freedom for signals (DFS) to estimate the amount of information contained in observations in the context of observing system experiments. In addition, the singular value decomposition method has also been widely used for channel selection (Prunet et al., 2010; Zhang et al., 2011; Wang et al., 2014). In 2017, Chang et al. (2017) selected a new set of Infrared Atmospheric Sounding Interferometer (IASI) channels using the channel score index (CSI). Richardson et al. (2018) selected 75 from 853 channels based on the high spectral-resolution oxygen A-band instrument on NASA's Orbiting Carbon Observatory-2 (OCO-2), using information content analysis to retrieve the cloud optical depth, cloud properties, and position.

Today's main methods for channel selection use only the weighting function to study appropriate numerical methods, such as the data precision matrix method (Menke, 1984), singular value decomposition method (Prunet et al., 2010; Zhang et al., 2011; Wang

et al., 2014), and the Jacobi method (Aires et al., 1999; Rabier et al., 2010). The use of the methods allows sensitive channels to be selected. The above-mentioned studies also take into account the sensitivity of each channel to atmospheric parameters during channel selection, while ignoring some factors that impact retrieval results. The accuracy of retrieval results depends not only on the channel weighting function but also on the channel noise, background field, and the retrieval algorithm.

~~Currently, Channel selection mostly uses the~~ information content ~~is~~  
~~often employed in channel selection. During retrieval, this~~  
~~method~~and delivers the largest amount of information for the selected  
channel combination during the retrieval (Rodgers, 1996; Du et al.,  
2008; He et al., 2012; Richardson et al., 2018).

This method has made great breakthroughs in both theory and practice, and the concept of information content itself does consider all the height dependencies of the kernel matrix  $K$  (Rodgers, 2000). However, earlier works have neglected the height dependencies of  $K$  for simplicity. This paper uses the atmospheric retrievable index (ARI) as the index, which is based on information content (Du et al., 2008; Richardson et al. 2018). Channel selection is made at different heights, and an effective channel selection scheme is proposed which fully considers various factors, including the influence of

different channels on the retrieval results at different heights. This ensures the best accuracy of the retrieval product when using the selected channel. In addition, statistical inversion comparison experiments are used to verify the effectiveness of the method.

## 2 Channel selection indicator, scheme and method

### 2.1 Channel selection indicator

According to the concept of information content, the information content contained in a selected channel of a hyperspectral instrument can be described as H (Rodgers, 1996; Rabier et al., 2010). The final expression of H is:

$$H = -\frac{1}{2} \ln |\hat{S} S_a^{-1}|$$

$$= -\frac{1}{2} \ln |(S_a - S_a K^T (K S_a K^T + S_\varepsilon)^{-1} K S_a) S_a^{-1}|, \quad (1)$$

where  $S_a$  is the error covariance matrix of the background or the estimated value of atmospheric profile,  $S_\varepsilon$  represents the observation error covariance matrix of each hyperspectral detector channel,  $\hat{S} = (S_a - S_a K^T (K S_a K^T + S_\varepsilon)^{-1} K S_a)$  denotes the covariance matrix after retrieval, K is the weighting function matrix.

In order to describe the accuracy of the retrieval results visually

and quantitatively, the atmospheric retrievable index (ARI),  $p$ , (Du et al., 2008) is defined as follows:

$$p = 1 - \exp\left(\frac{1}{2n} \ln|\hat{S}S_a^{-1}|\right), \quad (2)$$

Assuming that before and after the retrieval, the ratio of the root mean square error of each element in the atmospheric state vector is  $1-p$ , then  $|\hat{S}S_a^{-1}| = (1-p)^{2n}$  is derived. By inverting the equation, the ARI that is  $p$  can be obtained in Eq. (2), which indicates the relative portion of the error that is eliminated by retrieval. In fact, before and after retrieval, the ratio of the root mean square error of each element cannot be  $1-p$ . Therefore,  $p$  defined by Eq. (1) is actually an overall evaluation of the retrieval result.

## 2.2 Channel selection scheme

The principle of channel selection is to find the optimum channel combination after numbering the channels. This combination makes the information content,  $H$ , or the ARI defined in this paper as large as possible, in order to maintain the highest possible accuracy in the retrieval results.

Let there be  $M$  layers in the vertical direction of the atmosphere and  $N$  satellite channels. Selecting  $n$  from  $N$  channels, there will be

$C_N^n$  combinations in each layer, leading  $C_N^n$  calculations to get  $C_N^n$  kinds of  $p$  results. Furthermore, there are  $M$  layers in the vertical direction of the atmosphere. Therefore, the entire atmosphere must be calculated  $M \cdot C_N^n$  times. However, the calculation  $M \cdot C_N^n$  times will be particularly large, which makes this approach impractical in calculating  $p$  for all possible combinations. Therefore, it is necessary to design an effective calculation scheme, and such a scheme, i.e., a channel selection method, using iteration is proposed, called the “sequential absorption method” (Dudhia et al., 2002; Du et al., 2008). The method’s main function is to select (“absorb”) channels one by one, taking the channel with the maximum value of  $p$ . Through  $n$  iterations,  $n$  channels can be selected as the final channel combination. The steps are as follows:

(**I**) The expression of information content in a single channel:

First, we use only one channel for retrieval. A row vector,  $k$ , in the weighting function matrix,  $K$ , is a weighting function corresponding to the channel. After observation in this channel, the error covariance matrix is:

$$\hat{S} = S_a - S_a k^T (s_\varepsilon + k S_a k^T)^{-1} k S_a. \quad (3)$$

It should be noted that  $(s_\varepsilon + k S_a k^T)$  is a scalar value in Eq. (3), so Eq. (3) can be converted to:

$$\hat{S} = \left( I - \frac{S_a k^T k}{(s_\varepsilon + k S_a k^T)} \right) S_a = \left( I - \frac{(k S_a)^T k}{(s_\varepsilon + k (k S_a)^T)} \right) S_a. \quad (4)$$

Substituting Eq. (4) into Eq. (2) gives:

$$p = 1 - \exp\left(\frac{1}{2n} \ln\left(\left|I - \frac{(kS_a)^T k}{(s_\varepsilon + k(kS_a)^T)}\right|\right)\right). \quad (5)$$

(2II) Simplification of Eq. (5) for calculating the p matrix value:

Since  $S_a$  and  $S_\varepsilon$  are positive definite symmetric ~~matrixes,~~

~~it~~ matrices, they can be decomposed into  $S_a = (S_a^{1/2})^T (S_a^{1/2})$  and

$$S_\varepsilon = (S_\varepsilon^{1/2})^T (S_\varepsilon^{1/2}).$$

$$\text{Define } R = S_\varepsilon^{1/2} K S_a^{1/2}. \quad (6)$$

The matrix R can then be regarded as a weighting function matrix, normalized by the observed error and a priori uncertainty. A row vector of R,  $r = s_\varepsilon^{-1/2} k S_a^{1/2}$ , represents the normalized weighting function matrix of a single channel. Substituting r into Eq. (5) gives:

$$p = 1 - \exp\left(\frac{1}{2n} \ln\left(\left|I - \frac{r r^T}{1 + r^T r}\right|\right)\right). \quad (7)$$

For arbitrary row vectors, a and b, using the matrix property

$\det(I + a^T b) = 1 + b a^T$ , the new expression for p is:

$$p = 1 - \exp\left(\frac{1}{2n} \ln\left(1 - \frac{r^T r}{1 + r^T r}\right)\right)$$

$$\begin{aligned}
&= 1 - \exp\left(\frac{1}{2n} \ln\left(\frac{1}{1+r^T r}\right)\right) \\
&= 1 - \exp\left(-\frac{1}{2n} \ln(1 + r^T r)\right). \tag{8}
\end{aligned}$$

483

484 | (3III) Iteration in a single layer:

485 First, the iteration in a single layer requires the calculation of R.

486 | ~~According to~~Using  $S_a$ ,  $S_\varepsilon$ , K and Eq. (6), R can be calculated.

487 Second, using Eq. (8), p of each candidate channel can be calculated.

488 Moreover, the channel corresponding to maximum p is the selected

489 channel for this iteration. After a channel has been selected,

490 according to Eq. (3) we can use  $\hat{S}$  to get  $S_a$  for the next iteration.

491 Finally, channels which are not selected during this iteration are used

492 as the candidate channels for the next iteration.

493 When selecting n from N channels, it is necessary to calculate

494  $(N-n/2)n \approx Nn$  p values, which is much smaller than  $C_N^n$ . In addition

495 to high computational efficiency by using this method, another

496 advantage is that all channels can be recorded in the order in which

497 they are selected. In the actual application, if  $n'$  channels are

498 needed, and  $n' < n$ , we will not need to select the channel again,

499 but record the selected channel only.

500 | (4IV) Iteration for different altitudes:

501 Because satellite channel sensitivity varies with height, repeating

the iterative process of step (3III), selects the optimum channels at different heights. Assuming there are  $M$  layers in the atmosphere and selecting  $n$  from  $N$  channels, it is necessary to calculate  $M \cdot (N - n/2)n \approx M \cdot Nn$   $p$  values, a much smaller number than  $M \cdot C_N^n$ . In this way, different channel sets can be used to evaluate corresponding height in the retrieved profiles.

### 2.3 Statistical inversion method

The inversion methods for the atmospheric temperature profiles can be summarized in two categories: statistical inversion and physical inversion. Statistical inversion is essentially a linear regression model which uses a large number of satellite measurements and atmospheric parameters to match samples and calculate their correlation coefficient. Then, based on the correlation coefficient, the required parameters of the independent measurements obtained by the satellite are retrieved. Because the method does not directly solve the radiation transfer equation, it has the advantages of fast calculation speed. In addition, the solution is numerically stable, which makes it one of the highest precision methods (Chedin et al., 1985). Therefore, the statistical inversion method will be used for our channel selection experiment and a regression equation will be established.



According to an empirical orthogonal function, the atmospheric temperature (or humidity),  $T$ , and the brightness temperature,  $T_b$ , are expanded as:

$$T = T^* \cdot A, \quad (9)$$

$$T_b = T_b^* \cdot A, \quad (10)$$

where  $T^*$  and  $T_b^*$  are the eigenvectors of the covariance matrix of temperature (or humidity) and brightness temperature, respectively.  $A$  and  $B$  stand for the corresponding expansion coefficient vectors of temperature (humidity) and brightness temperature.

Using the least squares method and the orthogonal property, the coefficient conversion matrix,  $V$ , is introduced:

$$A = V \cdot B, \quad (11)$$

$$\text{where } V = AB^T(BB^T)^{-1}. \quad (12)$$

Using the orthogonality, we get:

$$B = (T_b^*)^T T_b, \quad (13)$$

546

547  $A = (T^*)^T T. \quad (14)$

548

549 For convenience, the anomalies of the state vector (atmospheric  
550 temperature),  $T$ , and the observation vector (brightness temperature),  
551  $T_b$ , are taken:

552

553  $\hat{T} = \bar{T} + \hat{T}' = \bar{T} + GT_b' = \bar{T} + G(T_b - \bar{T}_b), \quad (15)$

554

555 where  $\hat{T}$  stands for the retrieval atmospheric temperature.  $\bar{T}$  and  
556  $\bar{T}_b$  are the corresponding average values of the elements,  
557 respectively.  $\hat{T}'$  and  $T_b'$  represent the corresponding anomalies  
558 of the elements, respectively.

559 Assuming there are  $k$  sets of observations, a sample anomaly  
560 matrix with  $k$  vectors can be constructed:

561

562  $T' = (t_1', t_2', \dots, t_k'), \quad (16)$

563

564  $T_b' = (t_{b1}', t_{b2}', \dots, t_{bk}'). \quad (17)$

565

566 Define the inversion error matrix as:

567

$$\delta = \bar{T} - \hat{T} = \hat{T}' - T' . \quad (18)$$

The retrieval error covariance matrix is:

$$\begin{aligned} S_{\delta} &= \frac{1}{k-n-1} \delta \delta^T \\ &= \frac{1}{k-n-1} (T' - GT_b')(T' - GT_b')^T \\ &= \frac{k-1}{k-n-1} (S_e - G^T S_{xy} - S_{xy} G^T + GS_y G^T), \end{aligned} \quad (19)$$

where

$$\begin{aligned} S_e &= \frac{1}{k-1} T' T'^T, \\ S_y &= \frac{1}{k-1} T_b' T_b'^T, \\ S_{xy} &= \frac{1}{k-1} T' T_b'^T. \end{aligned} \quad (20)$$

$S_e$  stands for the sample covariance matrix of  $T$ ,  $S_y$  denotes the sample covariance matrix of  $T_b$ , and  $S_{xy}$  represents the covariance matrix of  $T$  and  $T_b$ . The elements on the diagonal of the error covariance matrix,  $S_{\delta}$ , represent the retrieval error variance of  $T$ . The matrix  $G$  that minimizes the overall error variance is the least squares coefficient matrix of the regression equation (15), which meets the criteria:

$$\delta^2 = \text{tr}(S_\delta) = \min. \quad (21)$$

Taking a derivative of Eq. (21) with respect to  $G$ ,  $\frac{\partial}{\partial G} \text{tr}(S_\delta) = 0 = (-2S_{xy} + 2GS_y)$ , which means that:

$$G = S_{xy}S_y^{-1}. \quad (22)$$

Substituting Eq. (22) into Eq. (15) finally gives the least squares solution as:

$$\hat{T} = \bar{T} + S_{xy}S_y^{-1}(T_b - \bar{T}_b). \quad (23)$$

It should be noted that the least squares solution obtained here aims to minimize the sum of the error variance for each element in the atmospheric state vector after retrieval for several times. At present, statistical multiple regression is widely used in the retrieval of atmospheric profiles based on atmospheric remote sensing data. As long as there are enough data,  $S_{xy}$  and  $S_y$  can be determined.

### 3. Channel selection experiment

#### 3.1 Data and model

The Atmospheric Infrared Sounder (AIRS) is primarily designed to measure the Earth's atmospheric water vapor and temperature profiles on a global scale (Aumann et al., 2003; ~~Hoffmann and Alexander, 2009~~; Susskind et al., 2003). AIRS is a continuously operating cross-track scanning sounder, consisting of a telescope that feeds an echelle spectrometer. The AIRS infrared spectrometer acquires 2378 spectral samples at a resolution  $\lambda/\Delta\lambda$ , ranging from 1086 to 1570, in three bands: 3.74  $\mu\text{m}$  to 4.61  $\mu\text{m}$ , 6.20  $\mu\text{m}$  to 8.22  $\mu\text{m}$ , and 8.8  $\mu\text{m}$  to 15.4  $\mu\text{m}$ . The footprint size is 13.5 km ~~at nadir~~ (~~Susskind et al., 2003~~). The spectral range includes 4.3  $\mu\text{m}$  and 15.5  $\mu\text{m}$  for important temperature observation and  $\text{CO}_2$ , 6.3  $\mu\text{m}$  for water vapor, and 9.6  $\mu\text{m}$  for ozone absorption bands (Menzel et al., 2018). The root mean square error (RMSE) of the measured radiation is better than 0.2 K (Susskind et al., 2003). Moreover, global atmospheric profiles can be detected every day. Due to radiometer noise and faults, there are currently only 2047 effective channels. However, compared with previous infrared detectors, AIRS boasts a significant improvement in both the number of channels and spectral resolution (Aumann, 1994; Huang et al., 2005; Li et al., 2005).

The root mean square error of an AIRS infrared channel is shown in Fig. 1, ~~with black spots, indicating that~~. The measurement error is

not below 0.2K for all the instrument channels ~~possess a~~  
~~measurement error of less than 0.2 K.~~ There are a few channels with  
extremely large measurement errors, which reduce the accuracy of  
prediction to some extent. Among them, some extremely large  
measurement errors reduce the accuracy of prediction to some extent  
(Susskind et al., 2003). At present, more than 300 channels have not  
been used because their errors exceed 1 K. If data from these  
channels were to be used for retrieval, the accuracy of the retrieval  
could be reduced. Therefore, it is necessary to select a group of  
channels to improve the calculation efficiency and retrieval quality.  
In this paper we study channel selection for temperature profile  
retrieval by AIRS.

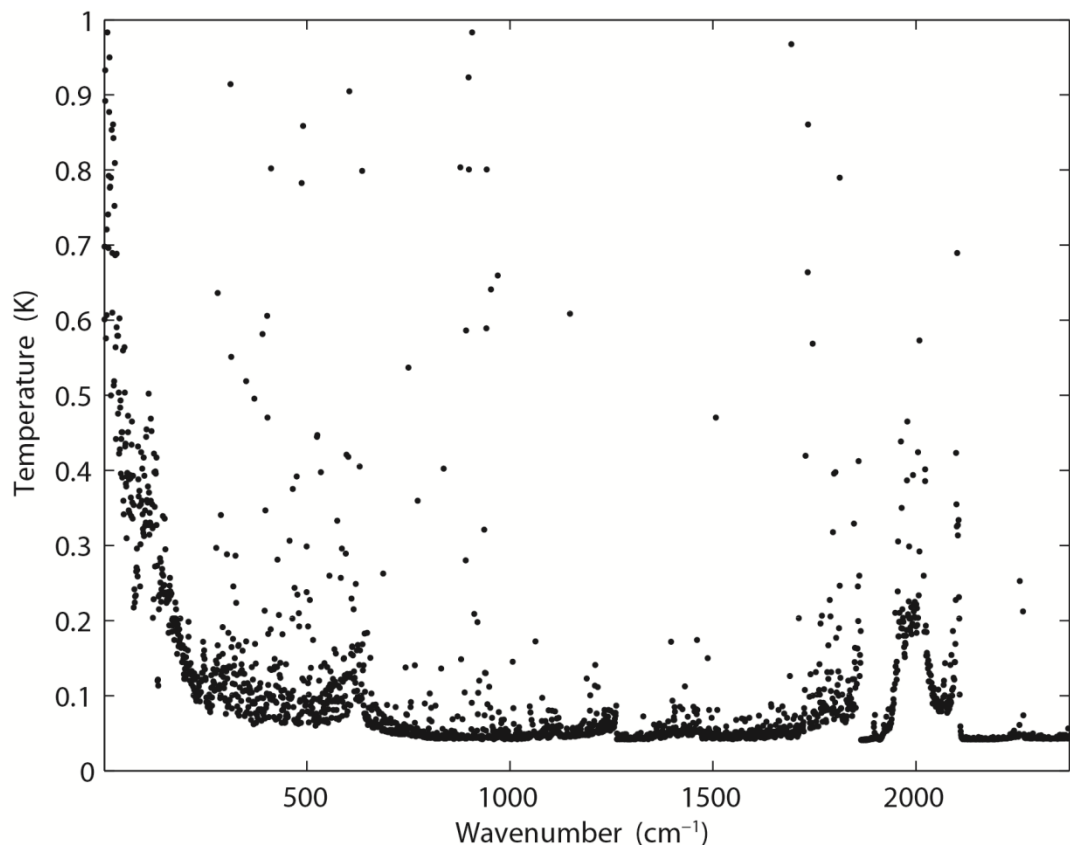


**Figure 1.** Root mean square error of AIRS infrared channel (black spots).

For the calculation of radiative transfer and the weighting function matrix,  $K$ , the RTTOV (Radiative Transfer for TOVS) v12 fast radiative transfer model is used. Although initially developed for the TOVS (TIROS Operational Vertical Sounder) radiometers, RTTOV can now simulate around 90 different satellite sensors measuring in the MW (microwave), IR (infrared) and VIS (visible) regions of the spectrum (Saunders et al., 2018). The model allows rapid simulations (1 ms for 40 channel ATOVS (Advanced TOVS) on a desktop PC) of radiances for satellite visible, infrared, or microwave nadir scanning radiometers given atmospheric profiles of temperature and trace gas concentrations, and cloud and surface properties. The only mandatory gas included as a variable for RTTOV v12 is water vapor. Optionally, ozone, carbon dioxide, nitrous oxide, methane, carbon monoxide, and sulfur dioxide can be included, with all other constituents assumed to be constant. RTTOV can accept input profiles on any defined set of pressure levels. The majority of RTTOV coefficient files are based on the 54 levels (see Table A1 in Appendix A), ranking in the range from 1050 hPa to 0.01 hPa, though coefficients for some hyperspectral sounders are also

available on 101 levels.

In order to correspond to the selected profiles, the atmosphere is divided into 137 layers, each of which contains corresponding atmospheric characteristics, such as temperature, pressure, and the humidity distribution. Each element in the weighting function matrix can be written as  $\partial y_i / \partial x_j$ . The subscript  $i$  is used to identify the satellite channel, and the subscript  $j$  is used to identify the atmospheric variable. Therefore,  $\partial y_i / \partial x_j$  indicates the variation in brightness temperature in a given satellite channel, when a given atmospheric variable in a given layer changes. We are thus able to establish which layer of the satellite channel is particularly sensitive to which atmospheric characteristic (temperature, various gas contents) in the vertical atmosphere. The RTTOV\_K (the K mode), is used to calculate the matrix  $H(X_0)$  (Eq. (1)) for a given atmospheric profile characteristic.

### **3.2 Channel selection comparison experiment and results**

In order to verify the effectiveness of the method, three sets of comparison experiments were conducted. First, 324 channels used by the EUMETSAT Satellite Application Facility on Numerical Weather Prediction (NWP SAF) were selected. NCS is short for NWP channel selection in this paper. NCS were released by the



NWPSAF 1DVar (one-dimensional variational analysis) scheme, in accordance with the requirements of the NWPSAF (Saunders et al., 2018). Second, 324 channels were selected using the information capacity method. This method was adopted by Du et al. (2008) without the consideration of layering. PCS is short for primary channel selection in this paper.

Third,  $324 \times M$  channels were selected using the information capacity method for the  $M$  layer atmosphere. ICS is short for improved channel selection in this paper. In order to verify the retrieval effectiveness after channel selection, statistical inversion comparison experiments were performed using 5000 temperature profiles provided by the ECMWF dataset, which will be introduced in Sect. 4.

The observation error covariance matrix,  $S_e$ , in the experiment is provided by NWP SAF 1Dvar. In general, it can be converted to a diagonal matrix, the elements of which are the observation error standard deviation of each hyperspectral detector channel, which is the square of the root mean square error for each channel. The root mean square error of the AIRS channels is shown in Fig. 1. The error covariance matrix of the background,  $S_a$ , is calculated using 5000 samples of the IFS-137 data provided by the ECMWF dataset (The detailed information will be introduced in Sect. 4). The last access

date is April 26th, 2019 (download address:  
<https://www.nwpsaf.eu/site/update-137-level-nwp-profile-dataset/>,  
2019). The covariance matrix of temperature is shown in Fig. 2. The  
results are consistent with the previous study by Du et al. (2008).

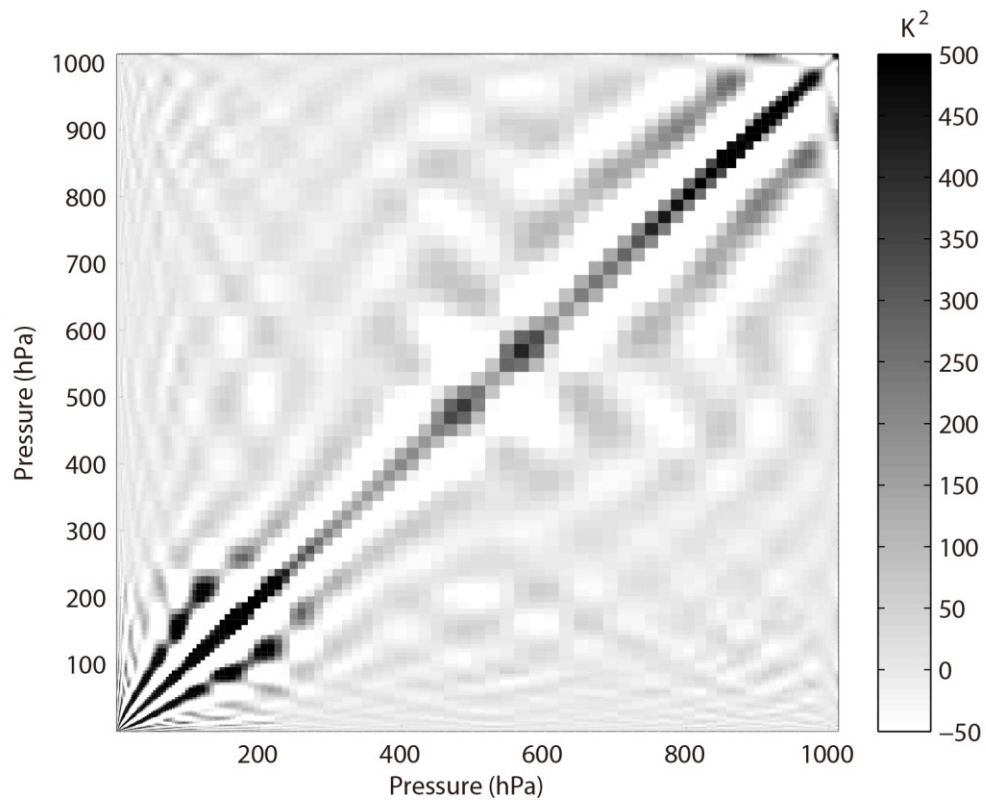


**Figure 2.** Error covariance matrix of temperature (shaded).

The reference atmospheric profiles are from the IFS-137 database,  
and the temperature weighting function matrix is calculated using  
the RTTOV\_K mode, as shown in Fig. 3; the results are consistent  
with those of the previous study by Du et al. (2008). For the  
air-based passive atmospheric remote sensing studied in this paper,

when the same channel detects the atmosphere from different observation angles, the value of the weighting function matrix  $K$  changes due to the limb effect. The goal of this section is focusing on the selection methods of selecting channels; therefore the biases produced from different observation angles can be ignored.

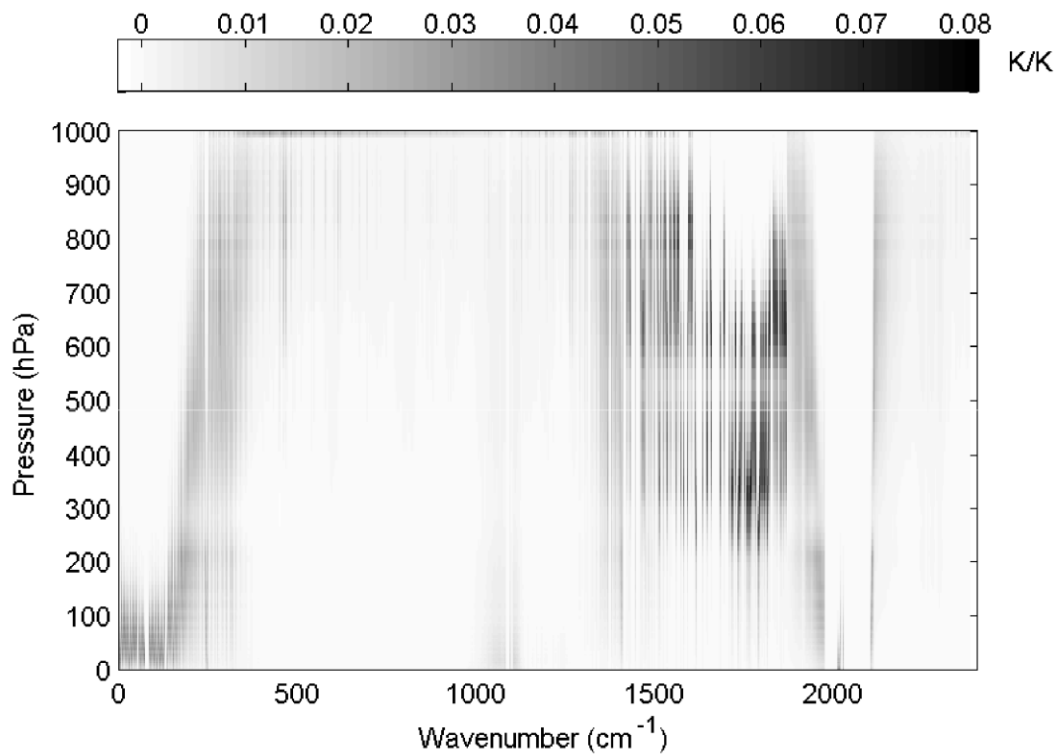


**Figure 3.** Temperature weighting function matrix (shaded).

In order to verify the effectiveness, the distribution of 324 channels, without considering layering, in the AIRS brightness temperature spectrum is indicated in Fig. 4. The background

736 brightness temperature is the simulated AIRS observation brightness  
737 temperature, which is from the atmospheric profile in RTTOV put  
738 into the model. Figure 4(a) shows the 324 channels selected by PCS,  
739 while Fig. 4(b) shows the 324 channels selected by NCS.

740

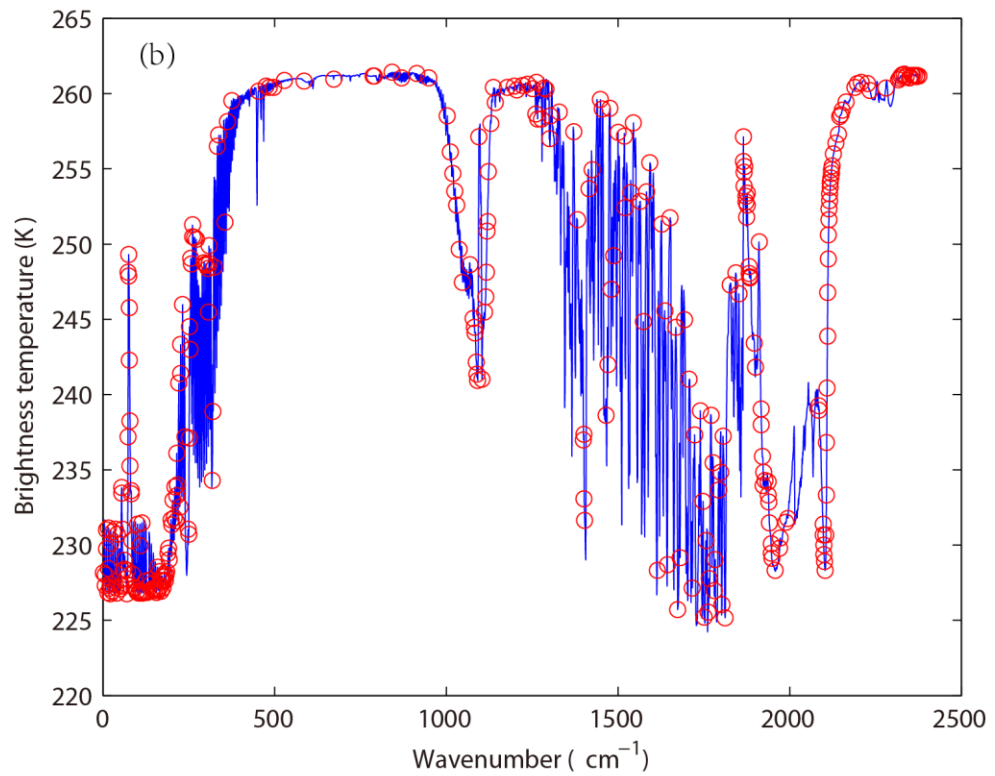
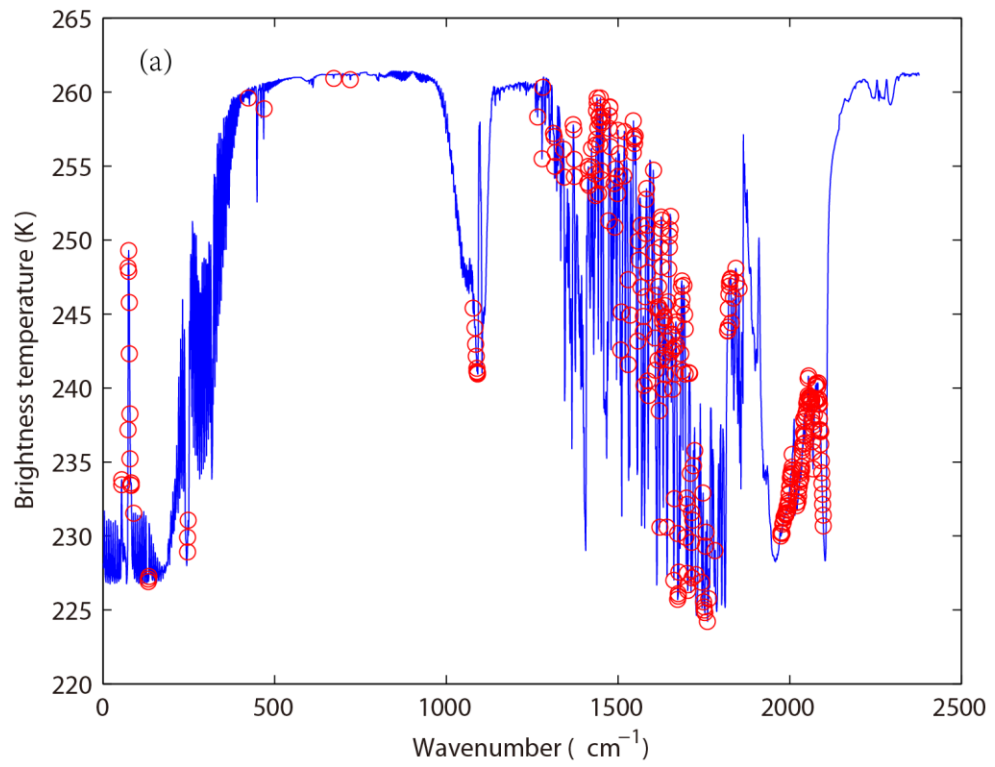


**Figure 4.** The distribution of different channel selection methods without considering layering in the AIRS brightness temperature

spectrum (blue line). (a) 324 channels selected by PCS (red circles).  
(b) 324 channels selected by NCS (red circles).

Without considering layering, the main differences between the 324 channels selected by PCS and NCS are as follows: (1) ~~When the wavenumber approaches 1000, the wavelength is 10  $\mu\text{m}$  ( $1/1000\text{-cm}^{-1}$ ).~~ Near 10  $\mu\text{m}$  band, fewer channels are selected by PCS because the retrieval of ground temperature is considered by NCS; (2) ~~When the wavenumber is near 1200, the wavelength is 9  $\mu\text{m}$  ( $1/1200\text{-cm}^{-1}$ ).~~ Near 9  $\mu\text{m}$  band, no channels are selected by PCS because the retrieval of O<sub>3</sub> is not considered in this paper; (3) ~~When the wavenumber approaches 1500, the wavelength is 6.7  $\mu\text{m}$  ( $1/1500\text{-cm}^{-1}$ ).~~ As is known, the spectral range from 6  $\mu\text{m}$  to 7  $\mu\text{m}$  corresponds to water vapor absorption bands, but fewer channels are selected by NCS; (4) ~~When the wavenumber is close to 2000, it derives a wavelength of 5  $\mu\text{m}$  ( $1/2000\text{-cm}^{-1}$ ), which~~ Near 5  $\mu\text{m}$  band, it includes 4.2  $\mu\text{m}$  for N<sub>2</sub>O and 4.3  $\mu\text{m}$  for CO<sub>2</sub> absorption bands. As is shown in Fig. 4, fewer channels are selected by PCS in those bands. PCS is favorable for atmospheric temperature observation ~~in the high temperature zone.~~ Because 4.2  $\mu\text{m}$  and 4.3  $\mu\text{m}$  bands are sensitive to high temperature, ~~the higher temperature is,~~ a better observation can be obtained for higher temperatures; (5) ~~In the near-infrared area, the wavenumber exceeds 2200, deriving a~~

~~wavelength of less than~~ Near  $4\text{ }\mu\text{m}$  ( $1/2000\text{-cm}^{-1}$ ). ~~Aband~~, a small number of channels is selected by NCS, but no channels are selected by PCS.

Above all, the information content ~~used~~ considered in this ~~paper~~ study only takes the temperature profile retrieval into consideration, so the channel combination of PCS is inferior to that of NCS for the retrieval of surface temperature and the  $\text{O}_3$  profile. The advantages of the channel selection method based on information content in this paper are mainly reflected in: (1) Stratosphere and mesosphere is less affected by the ground surface, so the retrieval result of PCS is better than that of NCS. (2) Due to the method selected in this paper there are more channels at  $4.2\text{ }\mu\text{m}$  for  $\text{N}_2\text{O}$  and  $4.3\text{ }\mu\text{m}$  for  $\text{CO}_2$  absorption bands; the channel combination of PCS is better than that of NCS for atmospheric temperature observation ~~to the~~ heat higher temperature.

By comparing channel selection without considering layering, we note the general advantages and disadvantages of PCS and NCS for the retrieval of temperature and can improve the channel selection scheme. First, the retrieval of the temperature profile for 324 channels selected by PCS is obtained. The relationship between the number of iterations and the ARI is shown in Fig. 5.





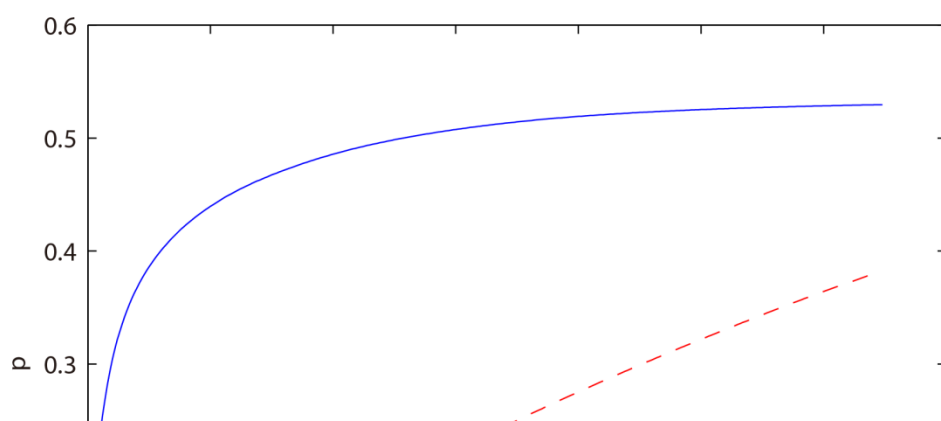
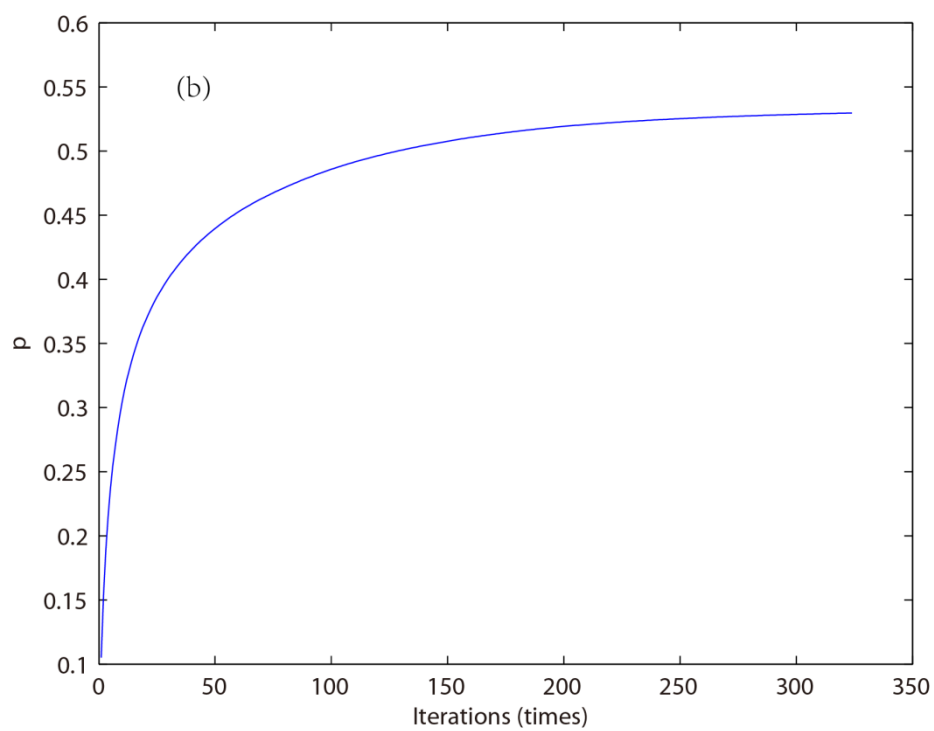
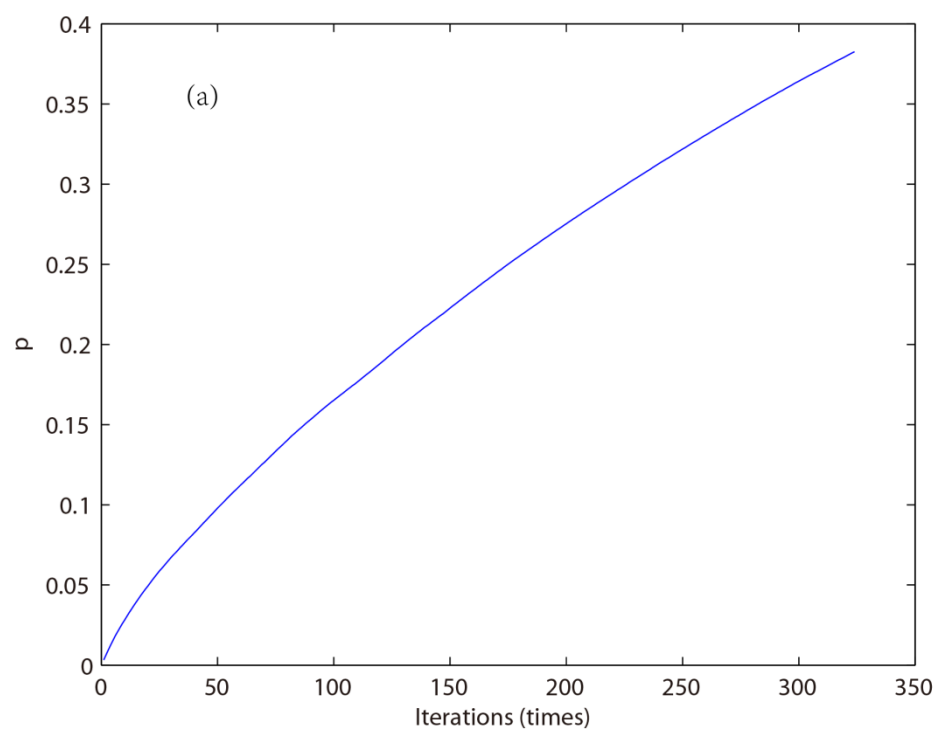
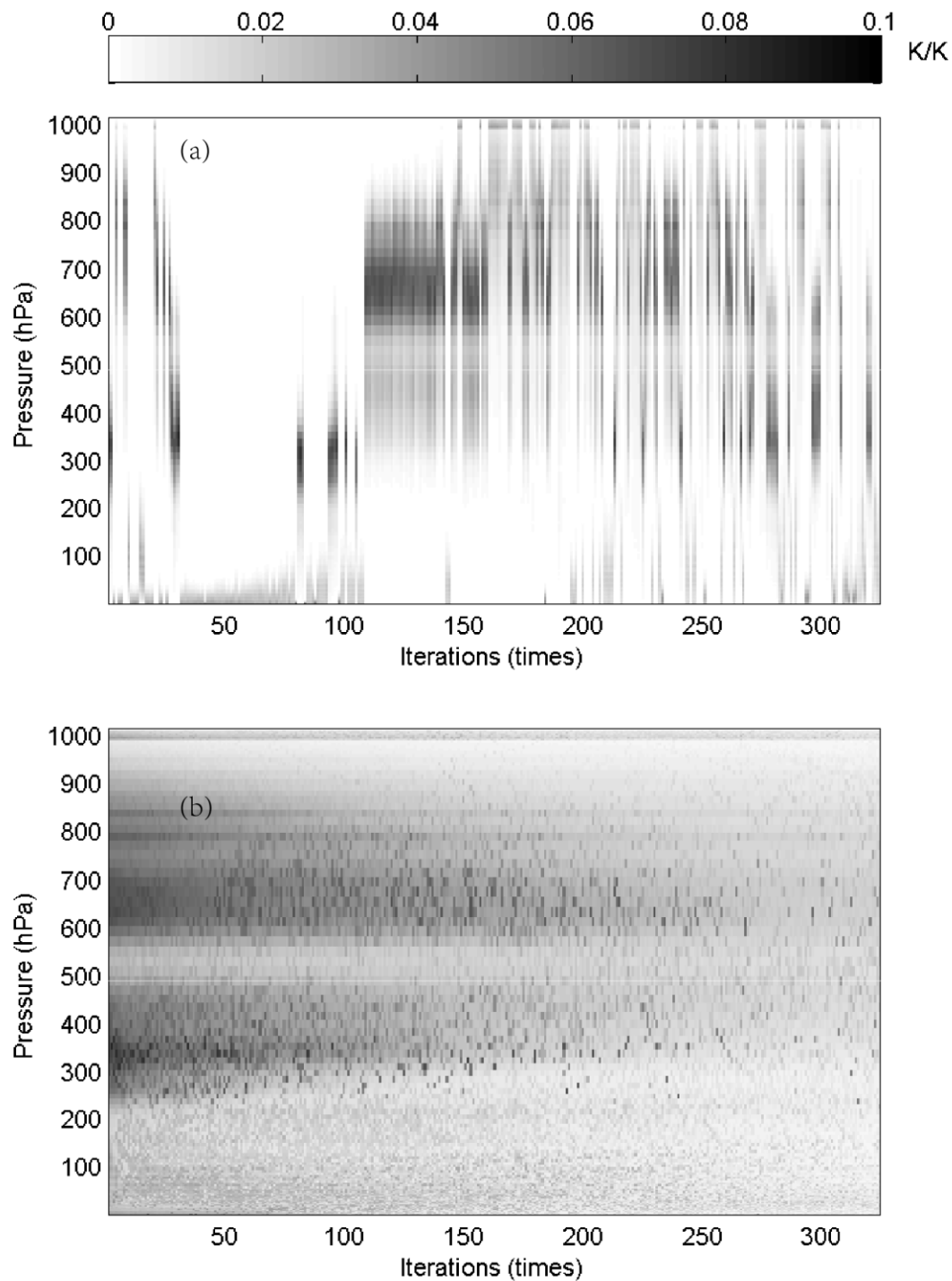


**Figure 5.** The relationship between the number of iterations and ARI.

~~(a)~~Blue line represents the result of ICS. Red dotted line stands for  
the result of PCS. ~~(b) ICS.~~

The ARI for PCS tends to be 0.38 and is not convergent, so the PCS method needs to be improved. In this paper, the atmosphere is divided into 137 layers, and based on the information content and iteration, 324 channels are selected for each layer. Then, the temperature profile of each layer can be retrieved based on statistical inversion (see at Sect. 4). The relationship between the number of iterations and the ARI for ICS is shown in Fig. 5b. When the number of iterations approaches 100, the ARI of ICS tends to be stable, and ~~reach to~~reaches 0.54. Thus, in terms of the ARI and convergence, the ICS method is better than that of PCS.

Furthermore, because an iterative method is used to select channels, the order of each selected channel is determined by the contribution from the ARI. The weighting function matrix of the top 324 selected channels, according to channel order, is shown in Fig. 6.



810 **Figure 6.** The relationship between the number of iterations and the  
811 weighting function of the top 324 selected channels (shaded). (a)  
812 ICS. (b) PCS.

As illustrated in Fig. 6, in the first 100 iterations, the distribution of the temperature weighting function for PCS is relatively scattered; it does not reflect continuity between the adjacent layers of the atmosphere. Besides, the ICS result is better than that of PCS, showing that: (1) the distribution of the temperature weighting function is more continuous and reflects the continuity between adjacent layers of the atmosphere; (2) regardless of the number of iterations, the maximum value of the weighting function is stable near 300–400 hPa and 600–700 hPa, without scattering, which is closer to the situation in real atmosphere.

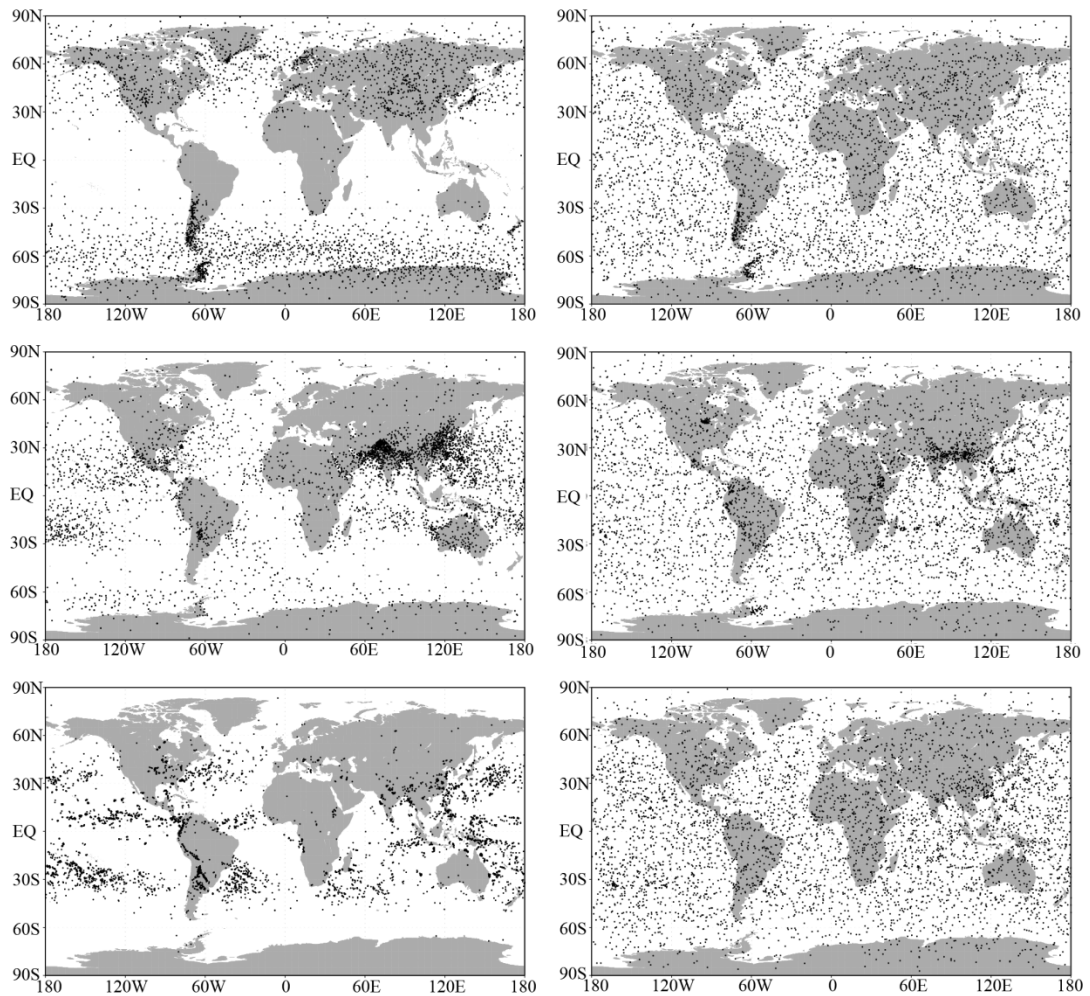
## **4. Statistical multiple regression experiment**

### **4.1 Temperature profile database**

A new database including a representative collection of 25,000 atmospheric profiles from the European Centre for Medium-range Weather Forecasts (ECMWF) was used for the statistical inversion experiments. The profiles were given in a 137-level vertical grid extending from the surface up to 0.01 hPa. The database was divided into five subsets focusing on diverse sampling characteristics such as temperature, specific humidity, ozone mixing ratio, cloud condensates, and precipitation. In contrast with earlier releases of the

ECMWF diverse profile database, the 137-level database places greater emphasis on preserving the statistical properties of sampled distributions produced by the Integrated Forecasting System (IFS) (Eresmaa and McNally, 2014; Brath et al., 2018). IFS-137 spans the period from September 1, 2013 to August 31, 2014. There are two operational analyses each day (at 00z and 12z), and approximately 13 000 atmospheric profiles over the ocean. The pressure levels adopted for IFS-137 are shown in Table A2 (see Table A2 in Appendix A).

The locations of selected profiles of temperature, specific humidity, and cloud condensate subsets of the IFS-91 and IFS-137 databases are plotted on the map in Fig. 7. In the IFS-91 database, the sampling is fully determined by the selection algorithm, which makes the geographical distributions very inhomogeneous. Selected profiles represent those regions where gradients of the sampled variable are the strongest: in the case of temperature, mid- and high-latitudes dominate, while humidity and cloud condensate subsets concentrate at low latitudes. However, the IFS-137 database shows a much more homogeneous spatial distribution in all the sampling subsets, which is a consequence of the randomized selection.



857 **Figure 7.** Locations of selected profiles in the temperature (top),  
 858 specific humidity (middle), and cloud condensate (bottom), sampled  
 859 subsets of the IFS-91 (left) and IFS-137 (right) databases (from  
 860 <https://www.nwpsaf.eu/site/update-137-level-nwp-profile-dataset/> ,  
 861 2019).

862

863 The temporal distribution of the selected profiles is illustrated in Fig.

864 8. The coverage of the IFS-137 data set is more homogeneous than

the IFS-91 data set. Moreover, the IFS-137 database supports the mode with input parameters, such as detection angle, 2 m temperature, and cloud information. Therefore, it is feasible to use the selected samples in a statistical multiple regression experiment.

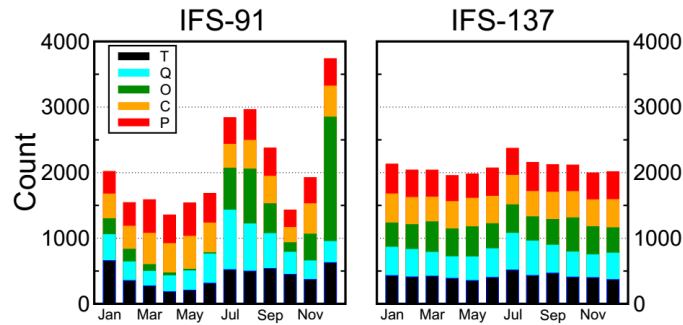


**Figure 8.** Distribution of profiles within the calendar months in IFS-91 (left) and IFS-137 (right) databases. Different subsets are shown in different colors. Black parts stand for temperature. Blue parts represent specific humidity. Green parts indicate ozone subset. Orange parts stand for cloud condensate. Red parts represent precipitation. The last access date is April 26th, 2019. (from <https://www.nwpsaf.eu/site/update-137-level-nwp-profile-dataset/>, 2019).

## 4.2 Experimental scheme

In order to verify the retrieval effectiveness of ICS, 5000 temperature profiles provided by the IFS-137 were used for statistical inversion comparison experiments. The steps are as follows:

(1) 5000 profiles and their corresponding surface factors, including surface air pressure, surface temperature, 2 m temperature, 2 m specific humidity, 10 m wind speed are put into the RTTOV mode. Then, the simulated AIRS spectra are obtained.

(2) The retrieval of temperature is carried out in accordance with Eq. (23). The 5000 profiles are divided into two groups. The first group of 2500 profiles is used to obtain the regression coefficient, and the second group of 2500 is used to test the result.

(3) Verification of the results. The test is carried out based on the standard deviation between the retrieval value and the true value.

### 4.3 Results and Discussion

For the statistical inversion comparison experiments, the standard deviation of temperature retrieval is shown in Fig. 9. First, because PCS does not take channel sensitivity as a function of height into consideration, the retrieval result of PCS is inferior to that of ICS. Second, by comparing the results of ICS and NCS we found that below 100 hPa, since the method used in this paper considers near ground to be less of an influencing factor, the channel combination of ICS is slightly inferior to that of NCS, but the difference is small.

From 100 hPa to 10 hPa, the retrieval temperature of ICS in this paper is consistent with that of NCS, slightly better than the channel



selected for NCS. From 10 hPa to 0.02 hPa, near the space layer, the retrieval temperature of ICS is better than that of NCS. In terms of the standard deviation, the channel combination of ICS is slightly better than that of PCS from 100 hPa to 10 hPa. From 10 hPa to 0.02 hPa, the standard deviation of ICS is lower than that of NCS at about 1 K, meaning that the retrieval result of ICS is better than that of NCS.

In order to further illustrate the effectiveness of ICS, the mean improvement value of the ICS and its percentages compared with the PCS and NCS at different heights are shown in Table 1. Because PCS does not take channel sensitivity as a function of height into consideration, the retrieval result of PCS is inferior to that of ICS. In general, the accuracy of the retrieval temperature of ICS is improved. Especially, from 100 hPa to 0.01 hPa, the mean value of ICS is evidently improved by more than 0.5 K which means the accuracy can be improved by more than 11%. By comparing the results of ICS and NCS we found that below 100 hPa, since the method used in this paper considers near ground to be less of an influencing factor, the channel combination of ICS is slightly inferior to that of NCS, but the difference is small. From 100 hPa to 0.01 hPa, the mean value of ICS is improved by more than 0.36 K which means the accuracy can be improved by more than 9.6%.

**Table 1.** The mean improvement value of the ICS and its percentages compared with the PCS and NCS at different heights.

Pressure	Improved mean value /Percentage compared with PCS	Improved value /Percentage compared with NCS
hPa	K/%	K/%
surface-100hPa	0.24/10.77%	-0.04/-3.27%
100hPa-10hPa	0.15/5.08%	0.06/2.4%
10hPa-1hPa	0.04/0.64%	0.17/2.99%
1hPa-0.01hPa	0.52/11.92%	0.36/9.57%

This is because, as shown in Fig. 4: (1) Stratosphere and mesosphere is less affected by the ground surface, so the retrieval result of PCS is better than that of NCS. (2) Due to the method selected in this paper, there are more channels at 4.2  $\mu\text{m}$  for  $\text{N}_2\text{O}$  and 4.3  $\mu\text{m}$  for  $\text{CO}_2$  absorption bands, and the channel combination of PCS is superior to that of NCS for atmospheric temperature observation in the high temperature zone. Moreover, ICS takes channel sensitivity as a function of height into consideration, so its retrieval result is improved.

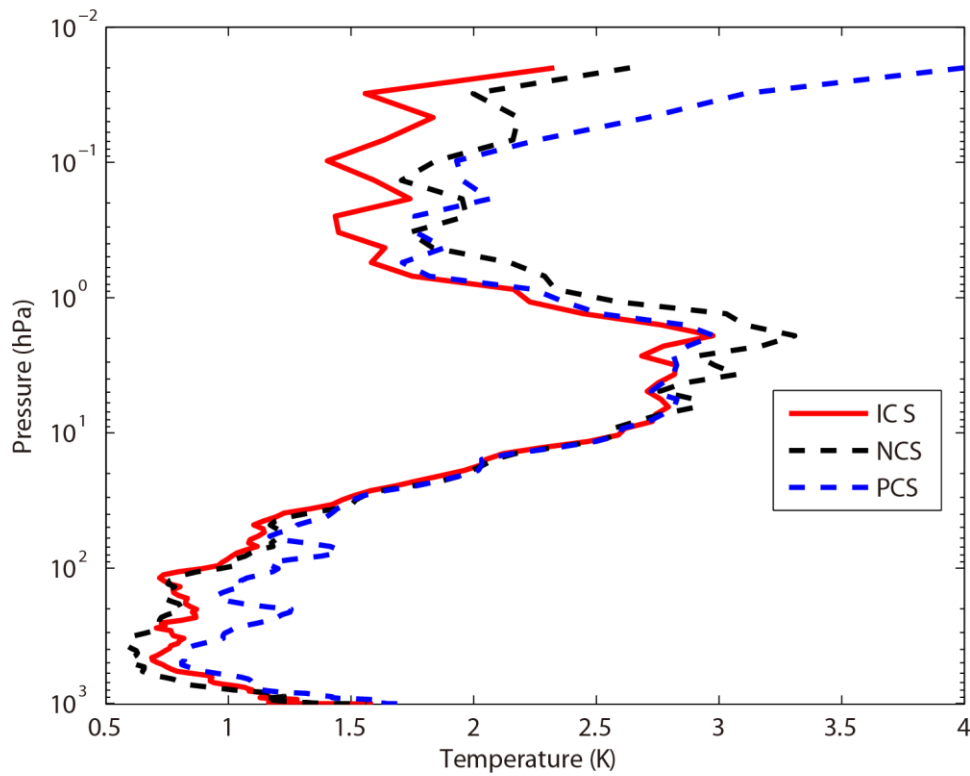


**Figure 9.** The temperature profile standard deviation of statistical inversion comparison experiments. Red line indicates the result of ICS. Black dotted line stands for the result of NCS. Blue dotted line represents the result of PCS.

## 5 Statistical inversion comparison experiments in four typical regions

The accuracy of the retrieval temperature varies from place to place and changes with atmospheric conditions. Therefore, in order to further compare the inversion accuracy under different atmospheric conditions, this paper has divided the atmospheric profile from the IFS-137 database introduced in Sect. 4 into four regions: equatorial

zone, subtropical region, mid-latitude region and Arctic. The average temperature profiles in these four regions are shown in Fig. 10. The retrieval temperature varies from place to place and changes with atmospheric conditions. In order to further compare the regional differences of inversion accuracy, the temperature standard deviations of ICS in four typical regions are compared in Sect. 5.2.

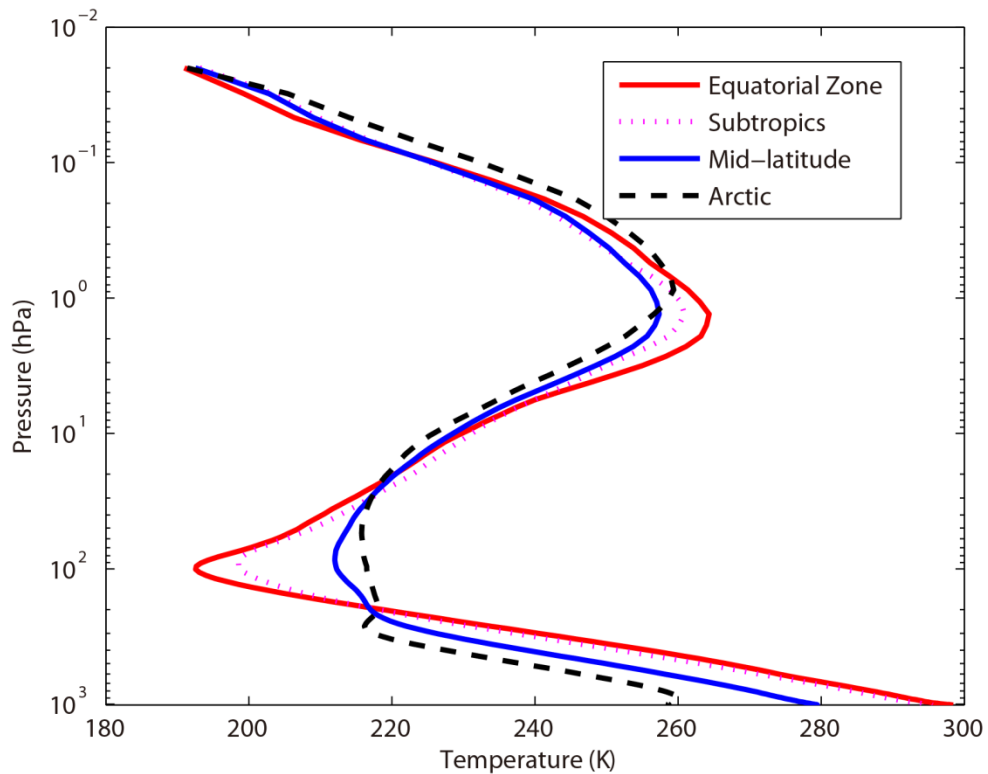


**Figure 10.** The average temperature profiles in four typical regions. Red line indicates the equatorial zone. Pink dotted line stands for the subtropics. Blue dotted line represents the mid-latitude region. Black dotted line stands for the Arctic.

## **5.1 Experimental scheme**

In order to further illustrate the different accuracy of the retrieval temperature using our improved channel selection method under different atmospheric conditions, the profiles in four typical regions were used for statistical inversion comparison experiments. The experimental steps are as follows:

(1) 2500 profiles in Sect. 4 are used to work out the regression coefficient.

(2) The atmospheric profiles of the four typical regions: equatorial zone, subtropical region, mid-latitude region and Arctic are used for statistical inversion comparison experiments and test the result.(3) Verification of the results. The test is carried out based on the standard deviation between the retrieval value and the true value.

## **5.2 Results and Discussion**

Using statistical inversion comparison experiments in four typical regions, the standard deviation of temperature retrieval is shown in Fig. 11. Generally, the retrieval temperature by ICS is better than that of NCS and PCS. In particular, above 1 hPa (the stratosphere and mesosphere), the standard deviation of atmospheric temperature can be improved by 1 K with PCS and NCS. Thus, ICS shows a

great improvement. The results were consistent with Sect. 4.

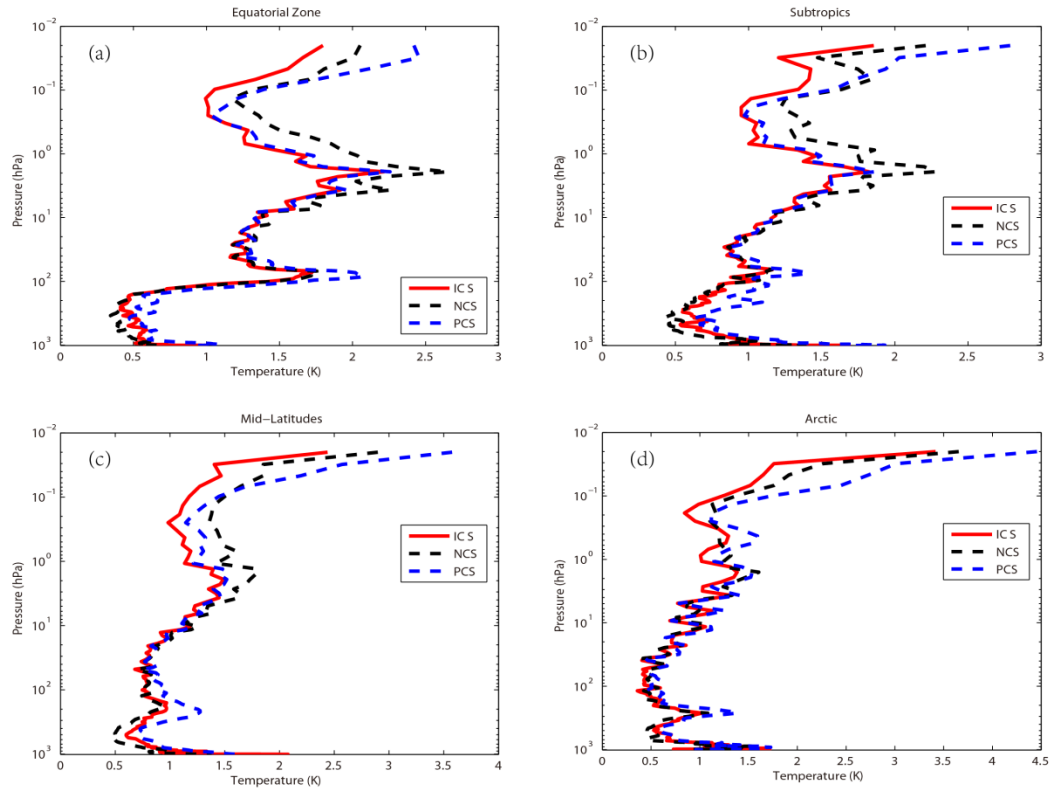


**Figure 11.** The temperature profile standard deviation of statistical inversion comparison experiments in four typical regions. Red line indicates the result of ICS. Black dotted line stands for the result of NCS. Blue dotted line represents the result of PCS. (a) Equatorial zone. (b) Subtropics. (c) Mid-latitudes. (d) Arctic.

In order to further compare the regional differences of inversion accuracy, the temperature standard deviation of ICS in four typical regions are compared in Fig. 12.

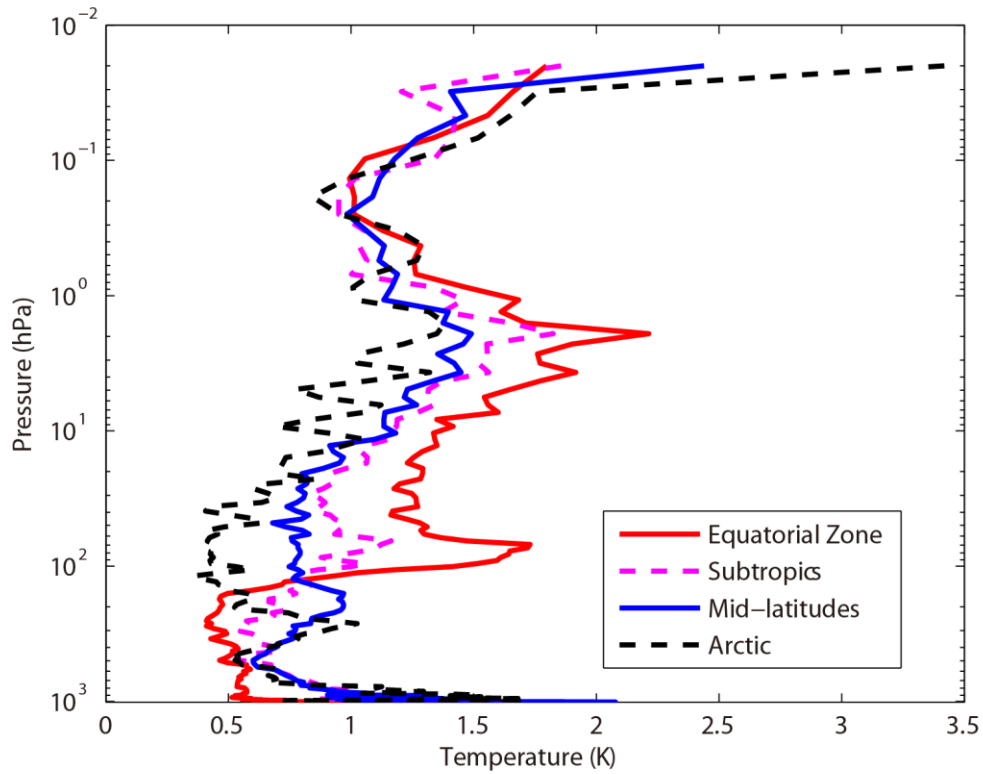


**Figure 12.** The temperature standard deviation of ICS in four typical regions. Red line indicates the result of equatorial zone. Pink dotted line represents the result of Subtropics. Blue line represents the result of Mid-latitudes. Black dotted line stands for the result of Arctic.

The temperature standard deviations of the ICS in the four typical regions are large (Fig. 12). Below 100 hPa, due to the high temperature in the equatorial zone, the channel combination of ICS is better than that of PCS and NCS for atmospheric temperature observation ~~to the~~ higher temperature. The standard deviation is 0.5K. Due to the method selected in this paper there are more

channels at 4.2  $\mu\text{m}$  for  $\text{N}_2\text{O}$  and 4.3  $\mu\text{m}$  for  $\text{CO}_2$  absorption bands which has been previously described in Sect. 3. Near the tropopause, the standard deviation of the equatorial zone increases sharply. It is also due to the sharp drops in temperature. However, the standard deviation of the Arctic is still around 0.5K. From 100hPa to 1hPa, the standard deviation of ICS is 0.5 K to 2K. With the increase of latitude, the effectiveness considerably increases. According to Fig. 11, ICS takes channel sensitivity as a function of height into consideration, so its retrieval result is better.

Although the improvements of ICS in the four typical regions are different, in general, the accuracy of the retrieval temperature of ICS is improved. Because PCS does not take channel sensitivity as a function of height into consideration, the retrieval result of PCS is inferior to that of ICS. In general, the accuracy of the retrieval temperature of ICS is improved.

## **7 Conclusions**

In recent years, the atmospheric layer in the altitude range of about 20–100 km has been named “the near space layer” by aeronautical and astronautical communities. It is between the space-based satellite platform and the aerospace vehicle platform, which is the transition zone between aviation and aerospace. Its unique resource



has attracted a lot of attention from many countries. Research and exploration, therefore, on and of the near space layer are of great importance. A new channel selection scheme and method for hyperspectral atmospheric infrared sounder AIRS data based on layering is proposed. The retrieval results of ICS concerning the near space atmosphere are particularly good. Thus, ICS aims to provide a new and an effective channel selection method for the study of the near space atmosphere using the hyperspectral atmospheric infrared sounder.

An improved channel selection method is proposed, based on information content in this paper. A robust channel selection scheme and method are proposed, and a series of channel selection comparison experiments are conducted. The results are as follows:

(1) Since ICS takes channel sensitivity as a function of height into consideration, the ARI of PCS only tends to be 0.38 and is not convergent. However, as the 100<sup>th</sup> iteration is approached, the ARI of ICS tends to be stable, reaching 0.54, while the distribution of the temperature weighting function is more continuous and closer to that of the actual atmosphere. Thus, in terms of the ARI, convergence, and the distribution of the temperature weighting function, ICS is better than PCS.

(2) Statistical inversion comparison experiments show that the

retrieval temperature of ICS in this paper is consistent with that of NCS. In particular, from 10 hPa to 0.02 hPa (the stratosphere and mesosphere), the retrieval temperature of ICS is obviously better than that of NCS at about 1 K. In general, the accuracy of the retrieval temperature of ICS is improved. Especially, from 100 hPa to 0.01 hPa, the accuracy of ICS can be improved by more than 11%. The reason is that stratosphere and mesosphere are less affected by the ground surface, so the retrieval result of ICS is better than that of NCS. Additionally, due to the method selected in this paper there are more channels at 4.2  $\mu\text{m}$  for the  $\text{N}_2\text{O}$  and at 4.3  $\mu\text{m}$  for the  $\text{CO}_2$  absorption bands; the channel combination of ICS is better than that of NCS for atmospheric temperature observation ~~to the~~at higher temperature.

(3) Statistical inversion comparison experiments in four typical regions indicate that ICS in this paper is significantly better than NCS and PCS in different regions and shows latitudinal variations, which shows potential for future applications.

*Data availability.* The data used in this paper are available from the corresponding author upon request.

*Appendices*

## Appendix A

**Table A1.** Pressure levels adopted for RTTOV v12 54 pressure level coefficients and profile limits within which the transmittance calculations are valid. Note that the gas units here are ppmv. (From <https://www.nwpsaf.eu/site/software/rttov/>, RTTOV Users guide, 2019).

Level	Pressure	Tmax	Tmin	Qmax	Qmin	Q <sub>2</sub> max	Q <sub>2</sub> min	Q <sub>2</sub> Ref
Number	hPa	K	K	ppmv*	ppmv*	ppmv*	ppmv*	ppmv*
1	0.01	245.95	143.66	5.24	0.91	1.404	0.014	0.296
2	0.01	252.13	154.19	6.03	1.08	1.410	0.069	0.321
3	0.03	263.71	168.42	7.42	1.35	1.496	0.108	0.361
4	0.03	280.12	180.18	8.10	1.58	1.670	0.171	0.527
5	0.13	299.05	194.48	8.44	1.80	2.064	0.228	0.769
6	0.23	318.64	206.21	8.59	1.99	2.365	0.355	1.074
7	0.41	336.24	205.66	8.58	2.49	2.718	0.553	1.471
8	0.67	342.08	197.17	8.34	3.01	3.565	0.731	1.991
9	1.08	340.84	189.50	8.07	3.30	5.333	0.716	2.787
10	1.67	334.68	179.27	7.89	3.20	7.314	0.643	3.756
11	2.50	322.5	176.27	7.75	2.92	9.191	0.504	4.864
12	3.65	312.51	175.04	7.69	2.83	10.447	0.745	5.953
13	5.19	303.89	173.07	7.58	2.70	12.336	1.586	6.763
14	7.22	295.48	168.38	7.53	2.54	12.936	1.879	7.109
15	9.84	293.33	166.30	7.36	2.46	12.744	1.322	7.060
16	13.17	287.05	163.47	7.20	2.42	11.960	0.719	6.574
17	17.33	283.36	161.49	6.96	2.20	11.105	0.428	5.687
18	22.46	280.93	161.47	6.75	1.71	9.796	0.278	4.705
19	28.69	282.67	162.09	6.46	1.52	8.736	0.164	3.870
20	36.17	279.93	162.49	6.14	1.31	7.374	0.107	3.111

21	45.04	27315	164.66	5.90	1.36	6.799	0.055	2.478
22	55.44	265.93	166.19	6.21	1.30	5.710	0.048	1.907
23	67.51	264.7	167.42	9.17	1.16	4.786	0.043	1.440
24	81.37	261.95	159.98	17.89	0.36	4.390	0.038	1.020
25	97.15	262.43	163.95	20.30	0.01	3.619	0.016	0.733
26	114.94	259.57	168.59	33.56	0.01	2.977	0.016	0.604
27	134.83	259.26	169.71	102.24	0.01	2.665	0.016	0.489
28	156.88	260.13	169.42	285.00	0.01	2.351	0.013	0.388
29	181.14	262.27	17063	714.60	0.01	1.973	0.010	0.284
30	207.61	264.45	174.11	1464.00	0.01	1.481	0.013	0.196
31	236.28	270.09	177.12	2475.60	0.01	1.075	0.016	0.145
32	267.10	277.93	181.98	4381.20	0.01	0.774	0.015	0.110
33	300.00	285.18	184.76	6631.20	0.01	0.628	0.015	0.086
34	334.86	293.68	187.69	9450.00	1.29	0.550	0.016	0.073
35	371.55	300.12	190.34	12432.00	1.52	0.447	0.015	0.063
36	409.89	302.63	194.40	15468.00	2.12	0.361	0.015	0.057
37	449.67	304.43	198.46	18564.00	2.36	0.284	0.015	0.054
38	490.85	307.2	201.53	21684.00	2.91	0.247	0.015	0.052
39	532.56	31217	202.74	24696.00	3.67	0.199	0.015	0.050
40	572.15	31556	201.61	27480.00	3.81	0.191	0.012	0.050
41	618.07	318.26	189.95	30288.00	6.82	0.171	0.010	0.049
42	661.00	321.71	189.95	32796.00	6.07	0.128	0.009	0.048
43	703.59	327.95	189.95	55328.00	6.73	0.124	0.009	0.047
44	745.48	333.77	189.95	37692.00	8.71	0.117	0.009	0.046
45	786.33	336.46	189.95	39984.00	8.26	0.115	0.008	0.045
46	825.75	338.54	189.95	42192.00	7.87	0.113	0.008	0.043
47	863.40	342.55	189.95	44220.00	7.53	0.111	0.007	0.041
48	898.93	346.23	189.95	46272.00	7.23	0.108	0.006	0.040
49	931.99	34924	189.95	47736.00	6.97	0.102	0.006	0.038
50	962.26	349.92	189.95	51264.00	6.75	0.099	0.006	0.034

51	989.45	350.09	189.95	49716.00	6.57	0.099	0.006	0.030
52	1013.29	360.09	189.95	47208.00	6.41	0.094	0.006	0.028
53	1033.54	350.09	189.95	47806.00	6.29	0.094	0.006	0.027
54	1050.00	350.09	189.95	47640.00	6.19	0.094	0.006	0.027

1087

1088 **Table A2.** Pressure levels adopted for IFS-137 137 pressure levels

1089 (in hPa).

Level number	pressure hPa	Level number	pressure hPa	Level number	pressure hPa	Level number	pressure hPa	Level number	pressure hPa
1	0.02	31	12.8561	61	106.4153	91	424.019	121	934.7666
2	0.031	32	14.2377	62	112.0681	92	441.5395	122	943.1399
3	0.0467	33	15.7162	63	117.9714	93	459.6321	123	950.9082
4	0.0683	34	17.2945	64	124.1337	94	478.3096	124	958.1037
5	0.0975	35	18.9752	65	130.5637	95	497.5845	125	964.7584
6	0.1361	36	20.761	66	137.2703	96	517.4198	126	970.9046
7	0.1861	37	22.6543	67	144.2624	97	537.7195	127	976.5737
8	0.2499	38	24.6577	68	151.5493	98	558.343	128	981.7968
9	0.3299	39	26.7735	69	159.1403	99	579.1926	129	986.6036
10	0.4288	40	29.0039	70	167.045	100	600.1668	130	991.023
11	0.5496	41	31.3512	71	175.2731	101	621.1624	131	995.0824
12	0.6952	42	33.8174	72	183.8344	102	642.0764	132	998.8081
13	0.869	43	36.4047	73	192.7389	103	662.8084	133	1002.225
14	1.0742	44	39.1149	74	201.9969	104	683.262	134	1005.356
15	1.3143	45	41.9493	75	211.6186	105	703.3467	135	1008.224
16	1.5928	46	44.9082	76	221.6146	106	722.9795	136	1010.849
17	1.9134	47	47.9915	77	231.9954	107	742.0855	137	1013.25
18	2.2797	48	51.199	78	242.7719	108	760.5996		
19	2.6954	49	54.5299	79	253.9549	109	778.4661		
20	3.1642	50	57.9834	80	265.5556	110	795.6396		
21	3.6898	51	61.5607	81	277.5852	111	812.0847		
22	4.2759	52	65.2695	82	290.0548	112	827.7756		
23	4.9262	53	69.1187	83	302.9762	113	842.6959		
24	5.6441	54	73.1187	84	316.3607	114	856.8376		
25	6.4334	55	77.281	85	330.2202	115	870.2004		
26	7.2974	56	81.6182	86	344.5663	116	882.791		
27	8.2397	57	86.145	87	359.4111	117	894.6222		
28	9.2634	58	90.8774	88	374.7666	118	905.7116		
29	10.372	59	95.828	89	390.645	119	916.0815		

*Author contributions.* ZS contributed the central idea. SC, ZS and HD conceived the method, developed the retrieval algorithm and discussed the results. SC analyzed the data, prepared the figures and wrote the paper. WG contributed to refining the ideas, carrying out additional analyses. All co-authors reviewed the paper.

*Competing interests.* The authors declare that they have no conflict of interest.

*Acknowledgements.* The study was supported by the National Key Research Program of China: Development of high-resolution data assimilation technology and atmospheric reanalysis data set in East Asia (Research on remote sensing telemetry data assimilation technology, Grant no. 2017YFC1501802). The study was also supported by the National Natural Science Foundation of China (Grant no. 41875045) and Hunan Provincial Innovation Foundation for Postgraduate (Grant no. CX2018B033 and no. CX2018B034).

## References

Aires, F., Schmitt, M., Chedin, A., and Scott, N.: The “weighting smoothing” regularization of MLP for Jacobian stabilization,

1111 IEEE. T. Neural. Networks., 10, 1502-1510,  
 1112 <https://doi.org/10.1109/72.809096>, 1999.

1113 Aires, F., Chédin, Alain., Scott, N. A., and Rossow, W. B.: A  
 1114 regularized neural net approach for retrieval of atmospheric and  
 1115 surface temperatures with the IASI instrument, J. Appl. Meteorol.,  
 1116 41,144-159,  
 1117 [https://doi.org/10.1175/1520-0450\(2002\)041<0144:ARNNAF>2.0](https://doi.org/10.1175/1520-0450(2002)041<0144:ARNNAF>2.0)  
 1118 .CO;2, 2002.

1119 Aumann, H. H.: Atmospheric infrared sounder on the earth  
 1120 observing system, Optl. Engr., 33, 776-784,  
 1121 <https://doi.org/10.1117/12.159325>, 1994.

1122 Aumann, H. H., Chahine, M. T., Gautier, C., and Goldberg, M.:  
 1123 AIRS/AMSU/HSB on the Aqua mission: design, science objective,  
 1124 data products, and processing systems, IEEE. Trans. GRS.,  
 1125 41,253-264, <http://dx.doi.org/10.1109/TGRS.2002.808356>, 2003.

1126 Brath, M., Fox, S., Eriksson, P., Harlow, R. C., Burgdorf, M., and  
 1127 Buehler, S. A.: Retrieval of an ice water path over the ocean from  
 1128 ISMAR and MARSS millimeter and submillimeter brightness  
 1129 temperatures, Atmos. Meas. Tech., 11, 611–632,  
 1130 <https://doi.org/10.5194/amt-11-611-2018>, 2018.

1131 Chahine, M. I.: A general relaxation method for inverse solution of  
 1132 the full radiative transfer equation, J. Atmos. Sci., 29, 741-747,

[https://doi.org/10.1175/1520-0469\(1972\)029<0741:AGRMFI>2.0.CO;2](https://doi.org/10.1175/1520-0469(1972)029<0741:AGRMFI>2.0.CO;2), 1972.

Chang, K. W, L'Ecuyer, T. S., Kahn, B. H., and Natraj, V.: Information content of visible and midinfrared radiances for retrieving tropical ice cloud properties, *J. Geophys. Res.*, 122, <https://doi.org/10.1002/2016JD026357>, 2017.

Chedin, A., Scott, N. A., Wahiche, C., and Moulinier, P.: The improved initialization inversion method: a high resolution physical method for temperature retrievals from satellites of the tiros-n series, *J. Appl. Meteor.*, 24, 128-143, [https://doi.org/10.1175/1520-0450\(1985\)024<0128:TIHIMA>2.0.CO;2](https://doi.org/10.1175/1520-0450(1985)024<0128:TIHIMA>2.0.CO;2), 1985.

Cyril, C., Alain, C., and Scott, N. A.: Airs channel selection for CO<sub>2</sub> and other trace-gas retrievals, *Q. J. Roy. Meteor. Soc.*, 129, 2719-2740, <https://doi.org/10.1256/qj.02.180>, 2003.

Du, H. D., Huang, S. X., and Shi, H. Q.: Method and experiment of channel selection for high spectral resolution data, *Acta. Physica. Sinica.*, 57, 7685-7692, 2008 .

Dudhia, A., Jay, V. L., and Rodgers, C. D.: Microwindow selection for high-spectral-resolution sounders, *Appl. Opt.* 41, 3665-3673, <https://doi.org/10.1364/AO.41.003665>, 2002.

Eresmaa, R. and McNally, A. P.: Diverse profile datasets from the



1155 ECMWF 137-level short-range forecasts, Tech. rep., ECMWF,  
 1156 2014.

1157 Eyre, J. R., Andersson E., and McNally, A. P.: Direct use of  
 1158 satellite sounding radiances in numerical weather prediction, High  
 1159 Spectral Resolution Infrared Remote Sensing for Earth's Weather  
 1160 and Climate Studies, Springer, Berlin, Heidelberg,  
 1161 [https://doi.org/10.1007/978-3-642-84599-4\\_25](https://doi.org/10.1007/978-3-642-84599-4_25), 1993.

1162 Fang, Z. Y.: The evolution of meteorological satellites and the  
 1163 insight from it, Adv. Meteorol. Sci. Technol., 4, 27-34,  
 1164 <https://doi.org/10.3969/j.issn.2095-1973.2014.06.003>, 2014.

1165 Gong, J., Wu, D. L., and Eckermann, S. D.: Gravity wave variances  
 1166 and propagation derived from AIRS radiances, Atmos. Chem.  
 1167 Phys., 11, 11691-11738,  
 1168 <https://doi.org/10.5194/acp-12-1701-2012>, 2011.

1169 He, M. Y., Du, H. D., Long, Z. Y., and Huang, S. X.: Selection of  
 1170 regularization parameters using an atmospheric retrievable index  
 1171 in a retrieval of atmospheric profile, Acta. Physica Sinica., 61,  
 1172 024205-160, 2012.

1173 Hoffmann, L. and Alexander, M. J.: Retrieval of stratospheric  
 1174 temperatures from atmospheric infrared sounder radiance  
 1175 measurements for gravity wave studies, J. Geophys. Res. Atm.,  
 1176 114, <https://doi.org/10.1029/2008JD011241>, 2009.

Huang, H. L., Li, J., Baggett, K., Smith, W. L., and Guan, L.:  
 Evaluation of cloud-cleared radiances for numerical weather  
 prediction and cloud-contaminated sounding applications,  
 Atmospheric and Environmental Remote Sensing Data Processing  
 and Utilization: Numerical Atmospheric Prediction and  
 Environmental Monitoring, I. S. O. Photonics.,  
<https://doi.org/10.1117/12.613027>, 2005.

Kuai, L., Natraj, V., Shia, R. L., Miller, C., and Yung, Y. L.: Channel  
 selection using information content analysis: a case study of CO<sub>2</sub>  
 retrieval from near infrared measurements. J. Q. S. Radiative.  
 Transfer., 111, 1296-1304,  
<https://doi.org/10.1016/j.jqsrt.2010.02.011>, 2010.

Li, J., Wolf, W. W., Menzel, W. P., Paul, Menzel. W., Zhang, W. J.,  
 Huang, H. L., and Achtor, T. H.: Global soundings of the  
 atmosphere from ATOVS measurements: the algorithm and  
 validation, J. Appl. Meteor., 39, 1248-1268,  
[https://doi.org/10.1175/1520-0450\(2000\)039<1248:GSOTAF>2.0.](https://doi.org/10.1175/1520-0450(2000)039<1248:GSOTAF>2.0.CO;2)  
 CO;2, 2000.

Li, J., Liu, C. Y., Huang, H. L., Schmit, T. J., Wu, X., Menzel, W. P.,  
 and Gurka, J. J.: Optimal cloud-clearing for AIRS radiances using  
 MODIS, IEEE. Trans. GRS. , 43, 1266-1278, [http://dx.doi.org/](http://dx.doi.org/10.1109/tgrs.2005.847795)  
[10.1109/tgrs.2005.847795](http://dx.doi.org/10.1109/tgrs.2005.847795), 2005.

- 1199 Liu, Z. Q.: A regional ATOVS radiance-bias correction scheme for  
 1200 radiance assimilation, *Acta. Meteorologica. Sinica.*, 65, 113-123,  
 1201 2007.
- 1202 Lupu, C., Gauthier, P., and Laroche, Stéphane.: Assessment of the  
 1203 impact of observations on analyses derived from observing system  
 1204 experiments, *Mon. Weather. Rev.*, 140, 245-257,  
 1205 <https://doi.org/10.1175/MWR-D-10-05010.1>, 2012.
- 1206 Menke, W.: *Geophysical Data Analysis: Discrete Inverse Theory*,  
 1207 Acad. Press., Columbia University, New York,  
 1208 <https://doi.org/10.1016/B978-0-12-397160-9.00019-9>, 1984.
- 1209 Menzel, W. P., Schmit, T. J., Zhang, P. and Li, J.: Satellite-based  
 1210 atmospheric infrared sounder development and applications, *Bull.*  
 1211 *Amer. Meteor. Soc.*, 99, 583–603,  
 1212 <https://doi.org/10.1175/BAMS-D-16-0293.1>, 2018.
- 1213 Prunet, P., Thépaut J. N., and Cass, V.: The information content of  
 1214 clear sky IASI radiances and their potential for numerical weather  
 1215 prediction, *Q. J. Roy. Meteor. Soc.*, 124, 211-241,  
 1216 <https://doi.org/10.1002/qj.49712454510>, 2010.
- 1217 Xu, Q.: Measuring information content from observations for data  
 1218 assimilation: relative entropy versus shannon entropy difference,  
 1219 *Tellus. A.*, 59, 198-209,  
 1220 <https://doi.org/10.1111/j.1600-0870.2006.00222.x>, 2007.

Rabier, F., Fourrié, N., and Chafai, D.: Channel selection methods for infrared atmospheric sounding interferometer radiances, Q. J. Roy. Meteor. Soc., 128, 1011-1027, <https://doi.org/10.1256/0035900021643638>, 2010.

Richardson, M. and Stephens, G. L.: Information content of oco-2 oxygen a-band channels for retrieving marine liquid cloud properties, Atmospheric Measurement Techniques, 11, 1-19, <https://doi.org/10.5194/amt-11-1515-2018>, 2018.

Rodgers, C. D.: Information content and optimisation of high spectral resolution remote measurements, Adv. Spa. Research, 21, 136-147, [https://doi.org/10.1016/S0273-1177\(97\)00915-0](https://doi.org/10.1016/S0273-1177(97)00915-0), 1996.

Rodgers, C. D.: Inverse Methods for Atmospheric Sounding, Inverse methods for atmospheric sounding, World Scientific, <https://doi.org/10.1142/3171>, 2000.

Saunders, R., Hocking, J., Turner, E., Rayer, P., Rundle, D., Brunel, P., Vidot, J., Roquet, P., Matricardi, M., Geer, A., Bormann, N., and Lupu, C.: An update on the RTTOV fast radiative transfer model (currently at version 12), Geosci. Model Dev., 11, 2717-2737, <https://doi.org/10.5194/gmd-11-2717-2018>, 2018.

Susskind, J., Barnett, C. D. and Blaisdell, J. M.: Retrieval of atmospheric and surface parameters from AIRS/AMSU/HSB data in the presence of clouds, IEEE Trans. Geosci. Remote Sensing,

1243 41, 390-409, <https://doi.org/10.1109/TGRS.2002.808236>, 2003.

1244 Smith, W. L., Woolf, H. M., and Revercomb, H. E.: Linear  
1245 simultaneous solution for temperature and absorbing constituent  
1246 profiles from radiance spectra, *Appl. Optics.*, 30, 1117,  
1247 <https://doi.org/10.1364/AO.30.001117>, 1991.

1248 Wakita, H., Tokura, Y., Furukawa, F., and Takigawa, M.: Study of  
1249 the information content contained in remote sensing data of  
1250 atmosphere, *Acta. Physica. Sinica.*, 59, 683-691, 2010.

1251 Wang, G., Lu, Q. F., Zhang, J. W., and Wang, H. Y.,.: Study on  
1252 method and experiment of hyper-spectral atmospheric infrared  
1253 sounder channel selection, *Remote Sensing Technology and*  
1254 *Application.*, 29, 795-802 , 2014.

1255 Zhang, J. W., Wang, G., Zhang, H., Huang J., Chen J., and Wu, L. L.:  
1256 Experiment on hyper-spectral atmospheric infrared sounder  
1257 channel selection based on the cumulative effect coefficient of  
1258 principal component, *Journal of Nanjing Institute of meteorology*,  
1259 1, 36-42, <http://dx.doi.org/10.3969/j.issn.1674-7097.2011.01.005>,  
1260 2011.

(c) The marked-up manuscript version

# A channel selection method for hyperspectral atmospheric infrared sounders based on layering

Shujie Chang<sup>1, 2, 3</sup>, Zheng Sheng<sup>1, 2</sup>, Huadong Du<sup>1, 2</sup>, Wei Ge<sup>1, 2</sup> and Wei Zhang<sup>1, 2</sup>

<sup>1</sup> College of Meteorology and Oceanography, National University of Defense Technology, Nanjing, China

<sup>2</sup> Collaborative Innovation Center on Forecast and Evaluation of Meteorological Disasters, Nanjing University of Information Science and Technology, Nanjing, China

<sup>3</sup> South China Sea Institute for Marine Meteorology, Guangdong Ocean University, Zhanjiang, China

**Correspondence:** Zheng Sheng (19994035@sina.com)

**Abstract.** This study introduces an effective channel selection method for hyperspectral infrared sounders. The method is illustrated for the Atmospheric InfraRed Sounder (AIRS) instrument. The results are as follows: (1) Using the improved channel selection (ICS), the atmospheric retrievable index is more stable, the value reaching 0.54. The coverage of the weighting functions is more

evenly distributed over height with this method; (2) Statistical inversion comparison experiments show that the accuracy of the retrieval temperature, using the improved channel selection method in this paper, is consistent with that of 1Dvar channel selection. In the stratosphere and mesosphere especially, from 10 hPa to 0.02 hPa, the accuracy of the retrieval temperature of our improved channel selection method is improved by about 1 K. Also at lower heights, the accuracy of the retrieval temperature of ICS is improved; (3) Statistical inversion comparison experiments for four different regions illustrate latitudinal and seasonal variations and better performance of ICS compared to the NWP Channel Selection (NCS) and Primary Channel Selection (PCS) methods. The ICS method shows potential for future applications.

## **1 Introduction**

Since the successful launch of the first meteorological satellite, TIROS in the 1960s, satellite observation technology has developed rapidly. Meteorological satellites observe the Earth's atmosphere from space and are able to record data from regions which are otherwise difficult to observe. Satellite data greatly enrich the content and range of meteorological observations, and consequently, atmospheric exploration technology and meteorological observations

have taken us to a new stage in our understanding of weather systems and related phenomena (Fang, 2014). From the perspective of vertical atmospheric observation, satellite instruments are developing rapidly. In their infancy, the traditional infrared measurement instruments for detecting atmospheric temperature and moisture profiles, such as TOVS (Smith et al., 1991) or HIRS in ATOVS (Chahine, 1972; Li et al., 2000; Liu, 2007), usually employed filter spectrometry. Even though such instruments have played an important role in improving weather prediction, it is difficult to continue to build upon improvements in terms of observation accuracy and vertical resolution due to the limitation of low spectral resolution. By using this kind of filter-based spectroscopic measurement instrument, therefore, it is difficult to meet today's needs in numerical weather prediction (Eyre et al., 1993; Prunet et al., 2010; Menzel et al., 2018). To meet this challenge, a series of plans for the creation of high-spectral resolution atmospheric measurement instruments has been executed in the United States and in Europe in recent years: One example is the AIRS (Atmospheric InfraRed Sounder) on the Earth Observation System, "Aqua", launched on May 4, 2002 from the United States. AIRS has 2378 spectral channels providing sensitivity from the ground to up to about 65 km of altitude (Aumann et al., 2003;



Hoffmann and Alexander, 2009; Gong et al., 2011). The United States and Europe, in 2010 and in 2007, also installed the CRIS (Cross-track Infrared Sounder) and the IASI (Infrared Atmospheric Sounding Interferometer) on polar-orbiting satellites.

China also devotes great importance to the development of such advanced sounding technologies. In the early 1990s, the National Satellite Meteorological Center began to investigate the principles and techniques of hyperspectral resolution atmospheric observations. China's development of interferometric atmospheric vertical detectors eventually led to the launch of Fengyun No. 3, on May 27, 2008, and Fengyun No. 4 on December 11, 2016, both of which were equipped with infrared atmospheric instruments. How best to use the hyperspectral resolution observation data obtained from these instruments, to obtain reliable atmospheric temperature and humidity profiles, is an active area of study in atmospheric inversion theory.

Due to technical limitations, only a limited number of channels could at first be built into the typical satellite instruments. In this case, channel selection generally involved controlling the channel weighting function by utilizing the spectral response characteristics of the channel (such as center frequency and bandwidth). With the development of measurement technology, increasing numbers of

hyperspectral detectors were carried on meteorological satellites. Due to the large number of channels and data supported by such instruments today (such as AIRS with 2378 channels and IASI with 8461 channels), it has proven extremely cumbersome to store, transmit, and process such data. Moreover, there is often a close correlation between the channels, causing an ill-posedness of the inversion, potentially compromising accuracy of the retrieval product based on hyperspectral resolution data.

However, hyperspectral detectors have many channels and provide real-time mode prediction systems with vast quantities of data, which can significantly improve prediction accuracy. But, if all the channels are used to retrieve data, the retrieval time considerably increases. Even more problematic are the glut of information produced, and the unsuitability of the calculations for real-time forecasting. Concurrently, the computer processing power must be large enough to meet the demands of simulating all the channels simultaneously within the forecast time. In order to improve the calculation efficiency and retrieval quality, it is very important to properly select a set of channels that can provide as much information as possible.

Many researchers have studied channel selection algorithms. Menke (1984) first chose channels using a data precision matrix method.

Aires et al. (1999) made the selection using the Jacobian matrix, which has been widely used since then (Aires et al., 2002; Rabier et al., 2010). Rodgers (2000) indicated that there are two useful quantities in measuring the information provided by the observation data: Shannon information content and degrees of freedom. The concept of information capacity then became widely used in satellite channel selection. In 2007, Xu (2007) compared the Shannon information content with the relative entropy, analyzing the information loss and information redundancy. In 2008, Du et al. (2008) introduced the concept of the atmospheric retrievable index (ARI) as a criterion for channel selection, and in 2010, Wakita et al. (2010) produced a scheme for calculating the information content of the various atmospheric parameters in remote sensing using Bayesian estimation theory. Kuai et al. (2010) analyzed both the Shannon information content and degrees of freedom in channel selection when retrieving CO<sub>2</sub> concentrations using thermal infrared remote sensing and indicated that 40 channels could contain 75% of the information from the total channels. Cyril et al. (2003) proposed the optimal sensitivity profile method based on the sensitivity of different atmospheric components. Lupu et al. (2012) used degrees of freedom for signals (DFS) to estimate the amount of information contained in observations in the context of observing system

experiments. In addition, the singular value decomposition method has also been widely used for channel selection (Prunet et al., 2010; Zhang et al., 2011; Wang et al., 2014). In 2017, Chang et al. (2017) selected a new set of Infrared Atmospheric Sounding Interferometer (IASI) channels using the channel score index (CSI). Richardson et al. (2018) selected 75 from 853 channels based on the high spectral-resolution oxygen A-band instrument on NASA's Orbiting Carbon Observatory-2 (OCO-2), using information content analysis to retrieve the cloud optical depth, cloud properties, and position.

Today's main methods for channel selection use only the weighting function to study appropriate numerical methods, such as the data precision matrix method (Menke, 1984), singular value decomposition method (Prunet et al., 2010; Zhang et al., 2011; Wang et al., 2014), and the Jacobi method (Aires et al., 1999; Rabier et al., 2010). The use of the methods allows sensitive channels to be selected. The above-mentioned studies also take into account the sensitivity of each channel to atmospheric parameters during channel selection, while ignoring some factors that impact retrieval results. The accuracy of retrieval results depends not only on the channel weighting function but also on the channel noise, background field, and the retrieval algorithm.

Channel selection mostly uses the information content and delivers the

largest amount of information for the selected channel combination during the retrieval (Rodgers, 1996; Du et al., 2008; He et al., 2012; Richardson et al., 2018).

This method has made great breakthroughs in both theory and practice, and the concept of information content itself does consider all the height dependencies of the kernel matrix  $K$  (Rodgers, 2000). However, earlier works have neglected the height dependencies of  $K$  for simplicity. This paper uses the atmospheric retrievable index (ARI) as the index, which is based on information content (Du et al., 2008; Richardson et al. 2018). Channel selection is made at different heights, and an effective channel selection scheme is proposed which fully considers various factors, including the influence of different channels on the retrieval results at different heights. This ensures the best accuracy of the retrieval product when using the selected channel. In addition, statistical inversion comparison experiments are used to verify the effectiveness of the method.

## **2 Channel selection indicator, scheme and method**

### **2.1 Channel selection indicator**

According to the concept of information content, the information content contained in a selected channel of a hyperspectral instrument can be described as  $H$  (Rodgers, 1996; Rabier et al., 2010). The final

expression of H is:

$$H = -\frac{1}{2} \ln |\hat{S} S_a^{-1}|$$

$$= -\frac{1}{2} \ln |(S_a - S_a K^T (K S_a K^T + S_\varepsilon)^{-1} K S_a) S_a^{-1}|, \quad (1)$$

where  $S_a$  is the error covariance matrix of the background or the estimated value of atmospheric profile,  $S_\varepsilon$  represents the observation error covariance matrix of each hyperspectral detector channel,  $\hat{S} = (S_a - S_a K^T (K S_a K^T + S_\varepsilon)^{-1} K S_a)$  denotes the covariance matrix after retrieval, K is the weighting function matrix.

In order to describe the accuracy of the retrieval results visually and quantitatively, the atmospheric retrievable index (ARI), p, (Du et al., 2008) is defined as follows:

$$p = 1 - \exp\left(\frac{1}{2n} \ln |\hat{S} S_a^{-1}|\right), \quad (2)$$

Assuming that before and after the retrieval, the ratio of the root mean square error of each element in the atmospheric state vector is 1-p, then  $|\hat{S} S_a^{-1}| = (1 - p)^{2n}$  is derived. By inverting the equation, the ARI that is p can be obtained in Eq. (2), which indicates the relative portion of the error that is eliminated by retrieval. In fact,

before and after retrieval, the ratio of the root mean square error of each element cannot be 1-p. Therefore, p defined by Eq. (1) is actually an overall evaluation of the retrieval result.

## **2.2 Channel selection scheme**

The principle of channel selection is to find the optimum channel combination after numbering the channels. This combination makes the information content, H, or the ARI defined in this paper as large as possible, in order to maintain the highest possible accuracy in the retrieval results.

Let there be M layers in the vertical direction of the atmosphere and N satellite channels. Selecting n from N channels, there will be  $C_N^n$  combinations in each layer, leading  $C_N^n$  calculations to get  $C_N^n$  kinds of p results. Furthermore, there are M layers in the vertical direction of the atmosphere. Therefore, the entire atmosphere must be calculated  $M \cdot C_N^n$  times. However, the calculation  $M \cdot C_N^n$  times will be particularly large, which makes this approach impractical in calculating p for all possible combinations. Therefore, it is necessary to design an effective calculation scheme, and such a scheme, i.e., a channel selection method, using iteration is proposed, called the “sequential absorption method” (Dudhia et al., 2002; Du et al., 2008). The method’s main function is to select (“absorb”) channels one by

one, taking the channel with the maximum value of p. Through n iterations, n channels can be selected as the final channel combination. The steps are as follows:

(I) The expression of information content in a single channel:

First, we use only one channel for retrieval. A row vector, k, in the weighting function matrix, K, is a weighting function corresponding to the channel. After observation in this channel, the error covariance matrix is:

$$\hat{S} = S_a - S_a k^T (s_\varepsilon + k S_a k^T)^{-1} k S_a. \quad (3)$$

It should be noted that  $(s_\varepsilon + k S_a k^T)$  is a scalar value in Eq. (3), so Eq. (3) can be converted to:

$$\hat{S} = \left( I - \frac{S_a k^T k}{(s_\varepsilon + k S_a k^T)} \right) S_a = \left( I - \frac{(k S_a)^T k}{(s_\varepsilon + k (k S_a)^T)} \right) S_a. \quad (4)$$

Substituting Eq. (4) into Eq. (2) gives:

$$p = 1 - \exp\left(\frac{1}{2n} \ln\left(\left| I - \frac{(k S_a)^T k}{(s_\varepsilon + k (k S_a)^T)} \right|\right)\right). \quad (5)$$

(II) Simplification of Eq. (5) for calculating the p value:

Since  $S_a$  and  $S_\varepsilon$  are positive definite symmetric matrices, they can be decomposed into  $S_a = (S_a^{1/2})^T (S_a^{1/2})$  and  $S_\varepsilon = (S_\varepsilon^{1/2})^T (S_\varepsilon^{1/2})$ .

$$\text{Define } R = S_\varepsilon^{1/2} K S_a^{1/2}. \quad (6)$$



1505

1506 The matrix  $R$  can then be regarded as a weighting function matrix,  
 1507 normalized by the observed error and a priori uncertainty. A row  
 1508 vector of  $R$ ,  $r = s_\varepsilon^{-1/2} k S_a^{1/2}$ , represents the normalized weighting  
 1509 function matrix of a single channel. Substituting  $r$  into Eq. (5) gives:

1510

$$1511 \quad p = 1 - \exp\left(\frac{1}{2n} \ln \left( \left| I - \frac{rr^T}{1+rr^T} \right| \right)\right). \quad (7)$$

1512

1513 For arbitrary row vectors,  $a$  and  $b$ , using the matrix property  
 1514  $\det(I + a^T b) = 1 + ba^T$ , the new expression for  $p$  is:

1515

$$\begin{aligned} p &= 1 - \exp\left(\frac{1}{2n} \ln \left( 1 - \frac{r^T r}{1 + r^T r} \right)\right) \\ 1516 \quad &= 1 - \exp\left(\frac{1}{2n} \ln \left( \frac{1}{1 + r^T r} \right)\right) \\ 1517 \quad &= 1 - \exp\left(-\frac{1}{2n} \ln(1 + r^T r)\right). \end{aligned} \quad (8)$$

1518

1519 (III) Iteration in a single layer:

1520 First, the iteration in a single layer requires the calculation of  $R$ .

1521 Using  $S_a$ ,  $S_\varepsilon$ ,  $K$  and Eq. (6),  $R$  can be calculated. Second, using Eq.  
 1522 (8),  $p$  of each candidate channel can be calculated. Moreover, the  
 1523 channel corresponding to maximum  $p$  is the selected channel for this  
 1524 iteration. After a channel has been selected, according to Eq. (3) we

can use  $\hat{S}$  to get  $S_a$  for the next iteration. Finally, channels which are not selected during this iteration are used as the candidate channels for the next iteration.

When selecting  $n$  from  $N$  channels, it is necessary to calculate  $(N-n/2)n \approx Nn$   $p$  values, which is much smaller than  $C_N^n$ . In addition to high computational efficiency by using this method, another advantage is that all channels can be recorded in the order in which they are selected. In the actual application, if  $n'$  channels are needed, and  $n' < n$ , we will not need to select the channel again, but record the selected channel only.

(IV) Iteration for different altitudes:

Because satellite channel sensitivity varies with height, repeating the iterative process of step (III), selects the optimum channels at different heights. Assuming there are  $M$  layers in the atmosphere and selecting  $n$  from  $N$  channels, it is necessary to calculate  $M \cdot (N - n/2)n \approx M \cdot Nn$   $p$  values, a much smaller number than  $M \cdot C_N^n$ . In this way, different channel sets can be used to evaluate corresponding height in the retrieved profiles.

## 2.3 Statistical inversion method

The inversion methods for the atmospheric temperature profiles can be summarized in two categories: statistical inversion and physical

inversion. Statistical inversion is essentially a linear regression model which uses a large number of satellite measurements and atmospheric parameters to match samples and calculate their correlation coefficient. Then, based on the correlation coefficient, the required parameters of the independent measurements obtained by the satellite are retrieved. Because the method does not directly solve the radiation transfer equation, it has the advantages of fast calculation speed. In addition, the solution is numerically stable, which makes it one of the highest precision methods (Chedin et al., 1985). Therefore, the statistical inversion method will be used for our channel selection experiment and a regression equation will be established.

According to an empirical orthogonal function, the atmospheric temperature (or humidity),  $T$ , and the brightness temperature,  $T_b$ , are expanded as:

$$T = T^* \cdot A, \quad (9)$$

$$T_b = T_b^* \cdot A, \quad (10)$$

where  $T^*$  and  $T_b^*$  are the eigenvectors of the covariance matrix of temperature (or humidity) and brightness temperature, respectively.

A and B stand for the corresponding expansion coefficient vectors of temperature (humidity) and brightness temperature.

Using the least squares method and the orthogonal property, the coefficient conversion matrix,  $V$ , is introduced:

$$A = V \cdot B, \quad (11)$$

$$\text{where } V = AB^T(BB^T)^{-1}. \quad (12)$$

Using the orthogonality, we get:

$$B = (T_b^*)^T T_b, \quad (13)$$

$$A = (T^*)^T T. \quad (14)$$

For convenience, the anomalies of the state vector (atmospheric temperature),  $T$ , and the observation vector (brightness temperature),  $T_b$ , are taken:

$$\hat{T} = \bar{T} + \hat{T}' = \bar{T} + GT_b' = \bar{T} + G(T_b - \bar{T}_b), \quad (15)$$

where  $\hat{T}$  stands for the retrieval atmospheric temperature.  $\bar{T}$  and

$\bar{T}_b$  are the corresponding average values of the elements,  
 respectively.  $\hat{T}'$  and  $T'_b$  represent the corresponding anomalies  
 of the elements, respectively.

Assuming there are k sets of observations, a sample anomaly  
 matrix with k vectors can be constructed:

$$T' = (t'_1, t'_2, \dots, t'_k), \quad (16)$$

$$T'_b = (t'_{b1}, t'_{b2}, \dots, t'_{bk}). \quad (17)$$

Define the inversion error matrix as:

$$\delta = \bar{T} - \hat{T} = \hat{T}' - T'. \quad (18)$$

The retrieval error covariance matrix is:

$$\begin{aligned} S_\delta &= \frac{1}{k-n-1} \delta \delta^T \\ &= \frac{1}{k-n-1} (T' - GT'_b)(T' - GT'_b)^T \\ &= \frac{k-1}{k-n-1} (S_e - G^T S_{xy} - S_{xy} G^T + GS_y G^T), \end{aligned} \quad (19)$$

where

$$\begin{aligned}
1612 \quad S_e &= \frac{1}{k-1} T' T' T, \\
1613 \quad S_y &= \frac{1}{k-1} T_b' T_b' T, \\
1614 \quad S_{xy} &= \frac{1}{k-1} T' T_b' T. \tag{20}
\end{aligned}$$

1615

1616  $S_e$  stands for the sample covariance matrix of  $T$ ,  $S_y$  denotes the  
1617 sample covariance matrix of  $T_b$ , and  $S_{xy}$  represents the covariance  
1618 matrix of  $T$  and  $T_b$ . The elements on the diagonal of the error  
1619 covariance matrix,  $S_\delta$ , represent the retrieval error variance of  $T$ .  
1620 The matrix  $G$  that minimizes the overall error variance is the least  
1621 squares coefficient matrix of the regression equation (15), which  
1622 meets the criteria:

1623

$$1624 \quad \delta^2 = \text{tr}(S_\delta) = \min. \tag{21}$$

1625

1626 Taking a derivative of Eq. (21) with respect to  $G$ ,  $\frac{\partial}{\partial G} \text{tr}(S_\delta) = 0 =$   
1627  $(-2S_{xy} + 2GS_y)$ , which means that:

1628

$$1629 \quad G = S_{xy} S_y^{-1}. \tag{22}$$

1630

1631 Substituting Eq. (22) into Eq. (15) finally gives the least squares  
1632 solution as:

$$\hat{T} = \bar{T} + S_{xy}S_y^{-1}(T_b - \bar{T}_b). \quad (23)$$

It should be noted that the least squares solution obtained here aims to minimize the sum of the error variance for each element in the atmospheric state vector after retrieval for several times. At present, statistical multiple regression is widely used in the retrieval of atmospheric profiles based on atmospheric remote sensing data. As long as there are enough data,  $S_{xy}$  and  $S_y$  can be determined.

### **3. Channel selection experiment**

#### **3.1 Data and model**

The Atmospheric Infrared Sounder (AIRS) is primarily designed to measure the Earth's atmospheric water vapor and temperature profiles on a global scale (Aumann et al., 2003; Susskind et al., 2003). AIRS is a continuously operating cross-track scanning sounder, consisting of a telescope that feeds an echelle spectrometer. The AIRS infrared spectrometer acquires 2378 spectral samples at a resolution  $\lambda/\Delta\lambda$ , ranging from 1086 to 1570, in three bands: 3.74  $\mu\text{m}$  to 4.61  $\mu\text{m}$ , 6.20  $\mu\text{m}$  to 8.22  $\mu\text{m}$ , and 8.8  $\mu\text{m}$  to 15.4  $\mu\text{m}$ . The footprint size is 13.5 km. The spectral range includes 4.3  $\mu\text{m}$  and 15.5  $\mu\text{m}$  for important temperature observation and  $\text{CO}_2$ , 6.3  $\mu\text{m}$  for

water vapor, and 9.6  $\mu\text{m}$  for ozone absorption bands (Menzel et al., 2018). The root mean square error (RMSE) of the measured radiation is better than 0.2 K (Susskind et al., 2003). Moreover, global atmospheric profiles can be detected every day. Due to radiometer noise and faults, there are currently only 2047 effective channels. However, compared with previous infrared detectors, AIRS boasts a significant improvement in both the number of channels and spectral resolution (Aumann, 1994; Huang et al., 2005; Li et al., 2005).

The root mean square error of an AIRS infrared channel is shown in Fig. 1. The measurement error is not below 0.2K for all the instrument channels. There are a few channels with extremely large measurement errors, which reduce the accuracy of prediction to some extent. Among them, some extremely large measurement errors reduce the accuracy of prediction to some extent (Susskind et al., 2003). At present, more than 300 channels have not been used because their errors exceed 1 K. If data from these channels were to be used for retrieval, the accuracy of the retrieval could be reduced. Therefore, it is necessary to select a group of channels to improve the calculation efficiency and retrieval quality. In this paper we study channel selection for temperature profile retrieval by AIRS.



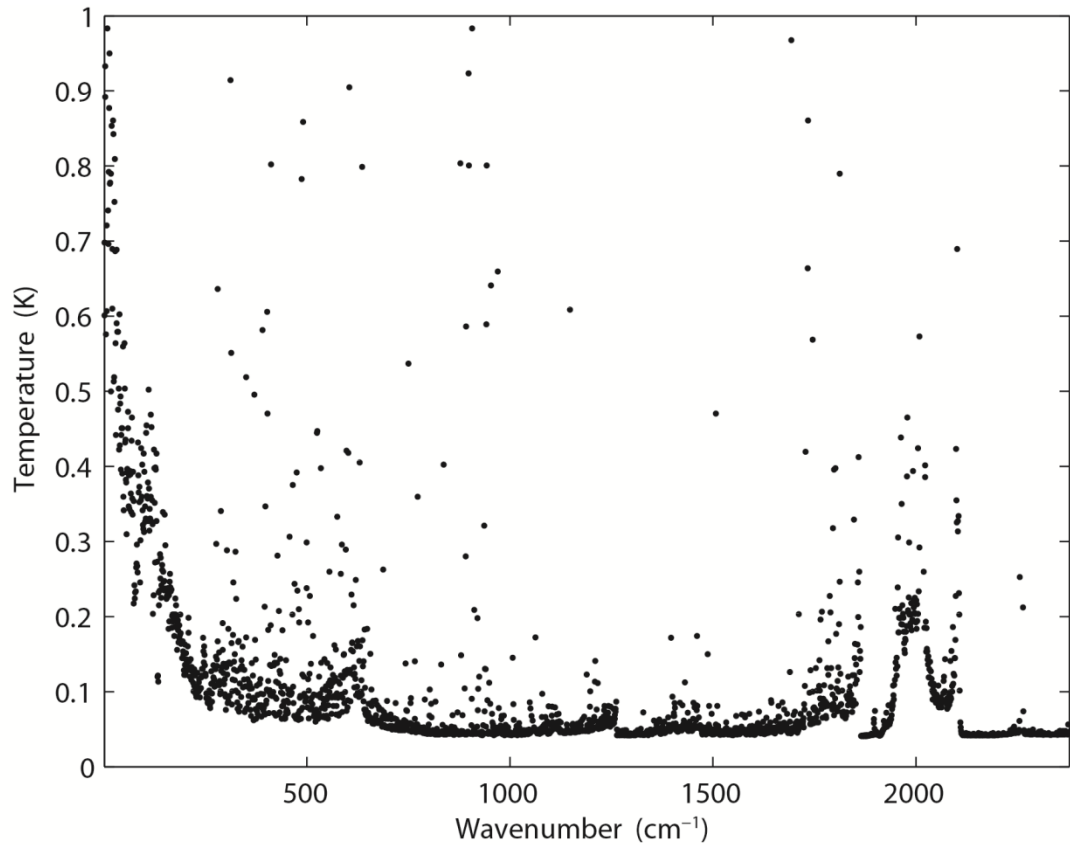


**Figure 1.** Root mean square error of AIRS infrared channel (black spots).

For the calculation of radiative transfer and the weighting function matrix,  $K$ , the RTTOV (Radiative Transfer for TOVS) v12 fast radiative transfer model is used. Although initially developed for the TOVS (TIROS Operational Vertical Sounder) radiometers, RTTOV can now simulate around 90 different satellite sensors measuring in the MW (microwave), IR (infrared) and VIS (visible) regions of the spectrum (Saunders et al., 2018). The model allows rapid simulations (1 ms for 40 channel ATOVS (Advanced TOVS) on a desktop PC) of radiances for satellite visible, infrared, or microwave

nadir scanning radiometers given atmospheric profiles of temperature and trace gas concentrations, and cloud and surface properties. The only mandatory gas included as a variable for RTTOV v12 is water vapor. Optionally, ozone, carbon dioxide, nitrous oxide, methane, carbon monoxide, and sulfur dioxide can be included, with all other constituents assumed to be constant. RTTOV can accept input profiles on any defined set of pressure levels. The majority of RTTOV coefficient files are based on the 54 levels (see Table A1 in Appendix A), in the range from 1050 hPa to 0.01 hPa, though coefficients for some hyperspectral sounders are also available on 101 levels.

In order to correspond to the selected profiles, the atmosphere is divided into 137 layers, each of which contains corresponding atmospheric characteristics, such as temperature, pressure, and the humidity distribution. Each element in the weighting function matrix can be written as  $\partial y_i / \partial x_j$ . The subscript  $i$  is used to identify the satellite channel, and the subscript  $j$  is used to identify the atmospheric variable. Therefore,  $\partial y_i / \partial x_j$  indicates the variation in brightness temperature in a given satellite channel, when a given atmospheric variable in a given layer changes. We are thus able to establish which layer of the satellite channel is particularly sensitive to which atmospheric characteristic (temperature, various gas

contents) in the vertical atmosphere. The RTTOV\_K (the K mode), is used to calculate the matrix  $H(X_0)$  (Eq. (1)) for a given atmospheric profile characteristic.

### **3.2 Channel selection comparison experiment and results**

In order to verify the effectiveness of the method, three sets of comparison experiments were conducted. First, 324 channels used by the EUMETSAT Satellite Application Facility on Numerical Weather Prediction (NWP SAF) were selected. NCS is short for NWP channel selection in this paper. NCS were released by the NWPSAF 1DVar (one-dimensional variational analysis) scheme, in accordance with the requirements of the NWPSAF (Saunders et al., 2018). Second, 324 channels were selected using the information capacity method. This method was adopted by Du et al. (2008) without the consideration of layering. PCS is short for primary channel selection in this paper.

Third,  $324 \times M$  channels were selected using the information capacity method for the M layer atmosphere. ICS is short for improved channel selection in this paper. In order to verify the retrieval effectiveness after channel selection, statistical inversion comparison experiments were performed using 5000 temperature profiles provided by the ECMWF dataset, which will be introduced

in Sect. 4.

The observation error covariance matrix,  $S_{\varepsilon}$ , in the experiment is provided by NWP SAF 1Dvar. In general, it can be converted to a diagonal matrix, the elements of which are the observation error standard deviation of each hyperspectral detector channel, which is the square of the root mean square error for each channel. The root mean square error of the AIRS channels is shown in Fig. 1. The error covariance matrix of the background,  $S_a$ , is calculated using 5000 samples of the IFS-137 data provided by the ECMWF dataset (The detailed information will be introduced in Sect. 4). The last access date is April 26th, 2019 (download address: <https://www.nwpsaf.eu/site/update-137-level-nwp-profile-dataset/>, 2019). The covariance matrix of temperature is shown in Fig. 2. The results are consistent with the previous study by Du et al. (2008).

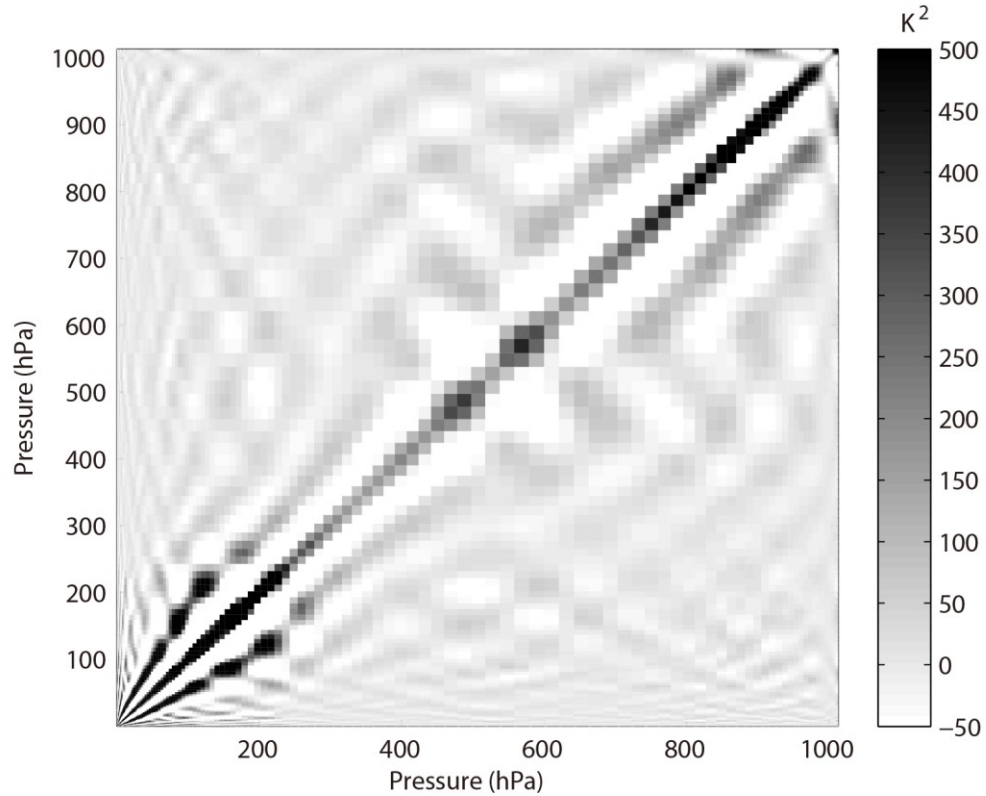


**Figure 2.** Error covariance matrix of temperature (shaded).

The reference atmospheric profiles are from the IFS-137 database, and the temperature weighting function matrix is calculated using the RTTOV\_K mode, as shown in Fig. 3; the results are consistent with those of the previous study by Du et al. (2008). For the air-based passive atmospheric remote sensing studied in this paper, when the same channel detects the atmosphere from different observation angles, the value of the weighting function matrix  $K$  changes due to the limb effect. The goal of this section is focusing on the selection methods of selecting channels; therefore the biases produced from different observation angles can be ignored.

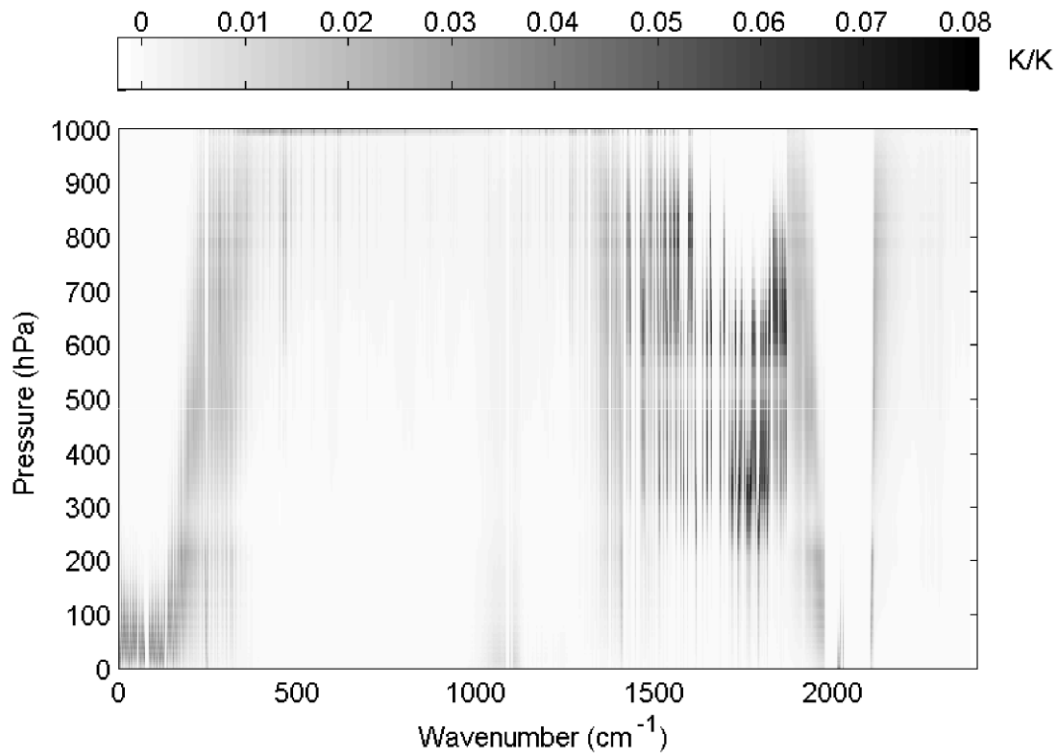
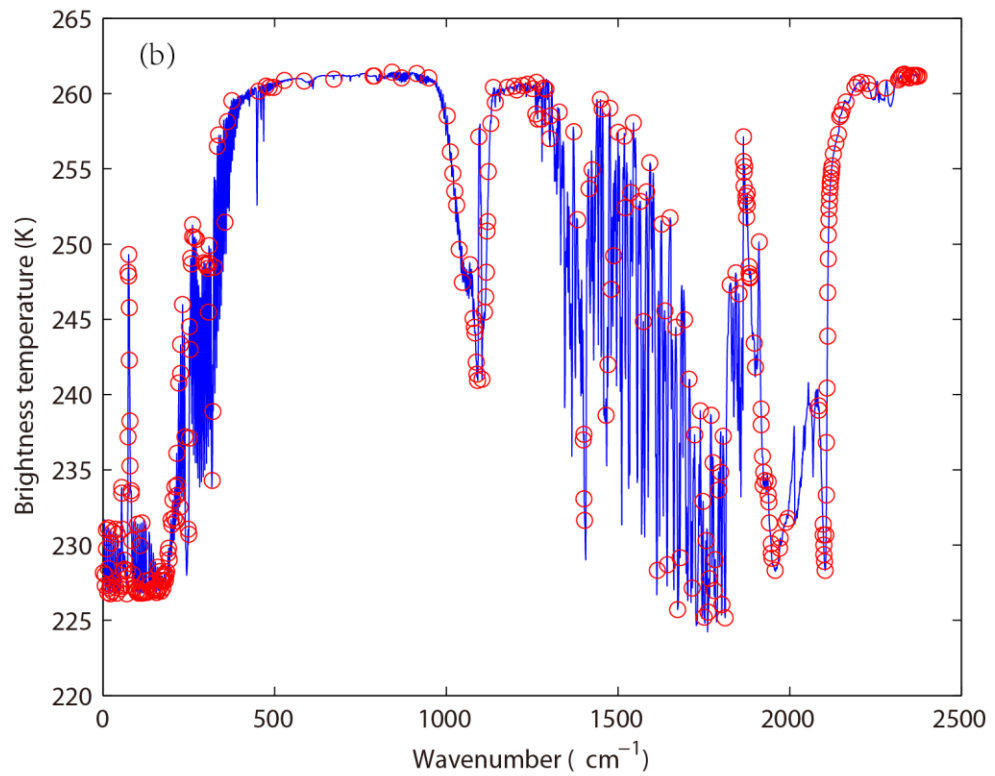
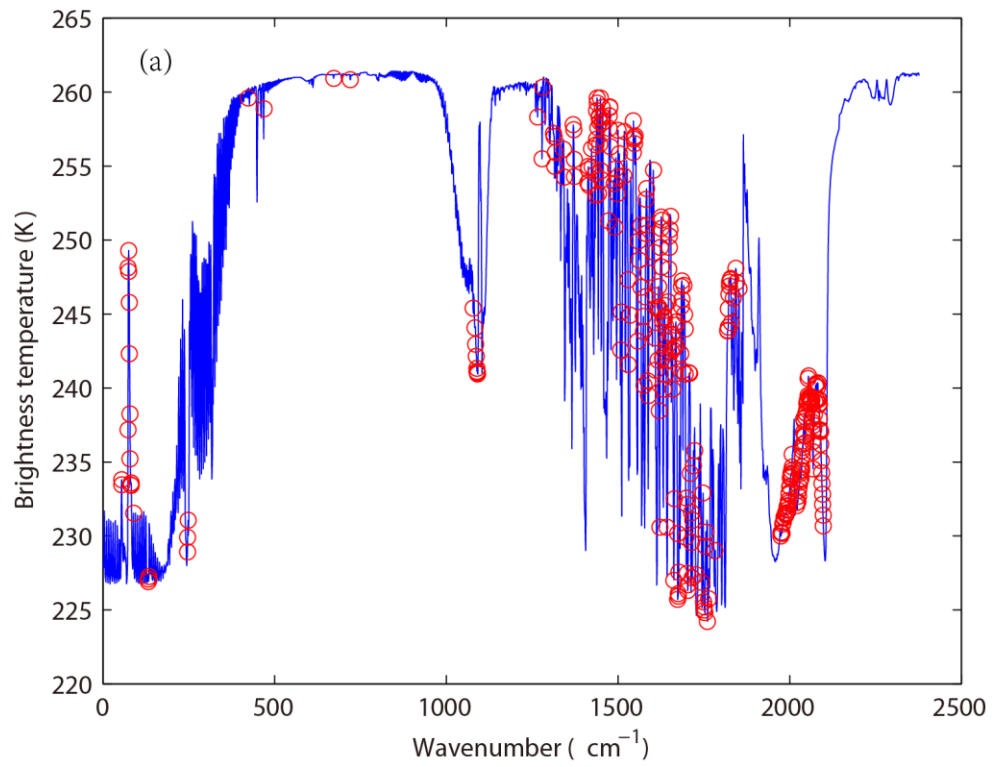


**Figure 3.** Temperature weighting function matrix (shaded).

In order to verify the effectiveness, the distribution of 324 channels, without considering layering, in the AIRS brightness temperature spectrum is indicated in Fig. 4. The background brightness temperature is the simulated AIRS observation brightness temperature, which is from the atmospheric profile in RTTOV put into the model. Figure 4(a) shows the 324 channels selected by PCS, while Fig. 4(b) shows the 324 channels selected by NCS.



1773

1774 **Figure 4.** The distribution of different channel selection methods

1775 without considering layering in the AIRS brightness temperature

spectrum (blue line). (a) 324 channels selected by PCS (red circles).  
(b) 324 channels selected by NCS (red circles).

Without considering layering, the main differences between the 324 channels selected by PCS and NCS are as follows: (1) Near 10  $\mu\text{m}$  band, fewer channels are selected by PCS because the retrieval of ground temperature is considered by NCS; (2) Near 9  $\mu\text{m}$  band, no channels are selected by PCS because the retrieval of  $\text{O}_3$  is not considered in this paper; (3) As is known, the spectral range from 6  $\mu\text{m}$  to 7  $\mu\text{m}$  corresponds to water vapor absorption bands, but fewer channels are selected by NCS; (4) Near 5  $\mu\text{m}$  band, it includes 4.2  $\mu\text{m}$  for  $\text{N}_2\text{O}$  and 4.3  $\mu\text{m}$  for  $\text{CO}_2$  absorption bands. As is shown in Fig. 4, fewer channels are selected by PCS in those bands. PCS is favorable for atmospheric temperature observation. Because 4.2  $\mu\text{m}$  and 4.3  $\mu\text{m}$  bands are sensitive to high temperature, a better observation can be obtained for higher temperatures; (5) Near 4  $\mu\text{m}$  band, a small number of channels is selected by NCS, but no channels are selected by PCS.

Above all, the information content considered in this study only takes the temperature profile retrieval into consideration, so the channel combination of PCS is inferior to that of NCS for the retrieval of surface temperature and the  $\text{O}_3$  profile. The advantages of the channel selection method based on information content in this



paper are mainly reflected in: (1) Stratosphere and mesosphere is less affected by the ground surface, so the retrieval result of PCS is better than that of NCS. (2) Due to the method selected in this paper there are more channels at 4.2  $\mu\text{m}$  for  $\text{N}_2\text{O}$  and 4.3  $\mu\text{m}$  for  $\text{CO}_2$  absorption bands; the channel combination of PCS is better than that of NCS for atmospheric temperature observation at higher temperature.

By comparing channel selection without considering layering, we note the general advantages and disadvantages of PCS and NCS for the retrieval of temperature and can improve the channel selection scheme. First, the retrieval of the temperature profile for 324 channels selected by PCS is obtained. The relationship between the number of iterations and the ARI is shown in Fig. 5.

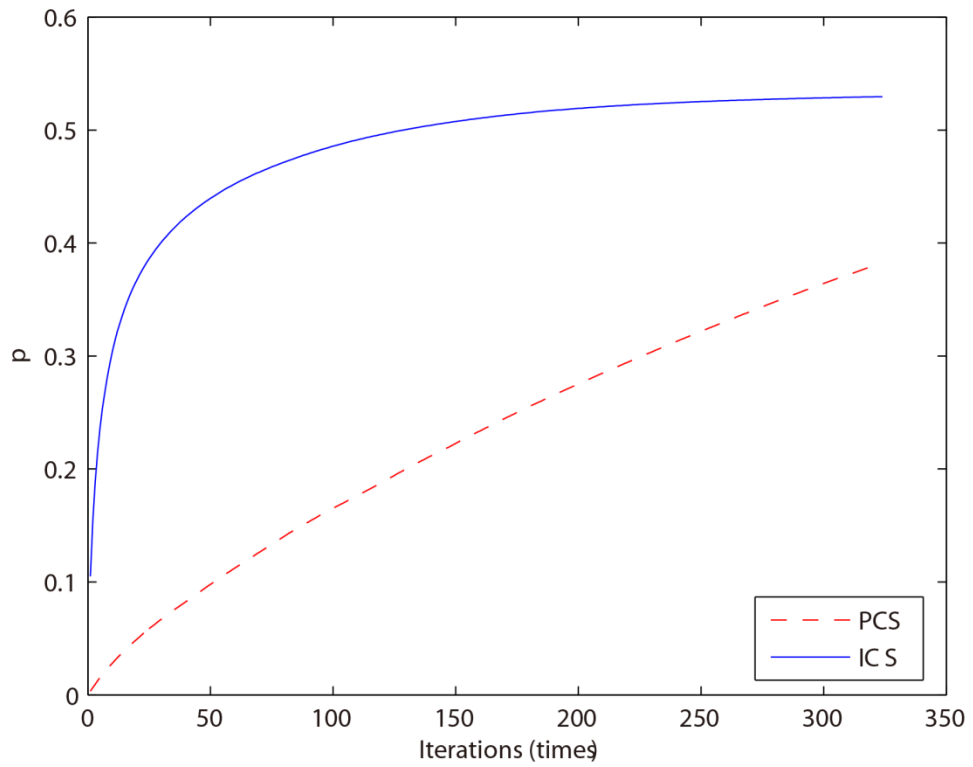
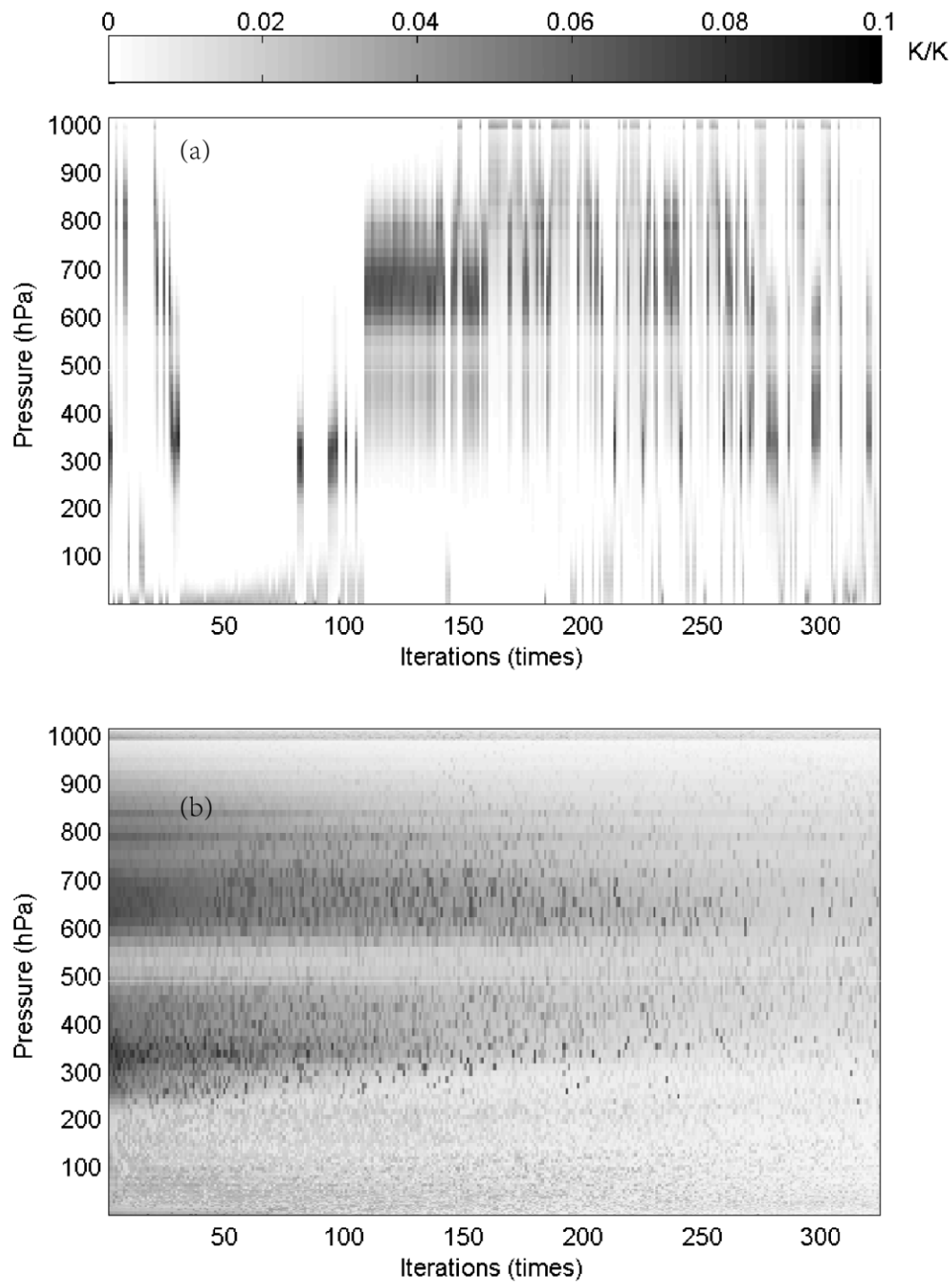


**Figure 5.** The relationship between the number of iterations and ARI. Blue line represents the result of ICS. Red dotted line stands for the result of PCS.

The ARI for PCS tends to be 0.38 and is not convergent, so the PCS method needs to be improved. In this paper, the atmosphere is divided into 137 layers, and based on the information content and iteration, 324 channels are selected for each layer. Then, the temperature profile of each layer can be retrieved based on statistical inversion (see at Sect. 4). The relationship between the number of iterations and the ARI for ICS is shown in Fig. 5b. When the number of iterations approaches 100, the ARI of ICS tends to be stable, and

1825 reaches 0.54. Thus, in terms of the ARI and convergence, the ICS  
1826 method is better than that of PCS.

1827 Furthermore, because an iterative method is used to select  
1828 channels, the order of each selected channel is determined by the  
1829 contribution from the ARI. The weighting function matrix of the top  
1830 324 selected channels, according to channel order, is shown in Fig.  
1831 6.



1833 **Figure 6.** The relationship between the number of iterations and the  
1834 weighting function of the top 324 selected channels (shaded). (a)  
1835 ICS. (b) PCS.

As illustrated in Fig. 6, in the first 100 iterations, the distribution of the temperature weighting function for PCS is relatively scattered; it does not reflect continuity between the adjacent layers of the atmosphere. Besides, the ICS result is better than that of PCS, showing that: (1) the distribution of the temperature weighting function is more continuous and reflects the continuity between adjacent layers of the atmosphere; (2) regardless of the number of iterations, the maximum value of the weighting function is stable near 300–400 hPa and 600–700 hPa, without scattering, which is closer to the situation in real atmosphere.

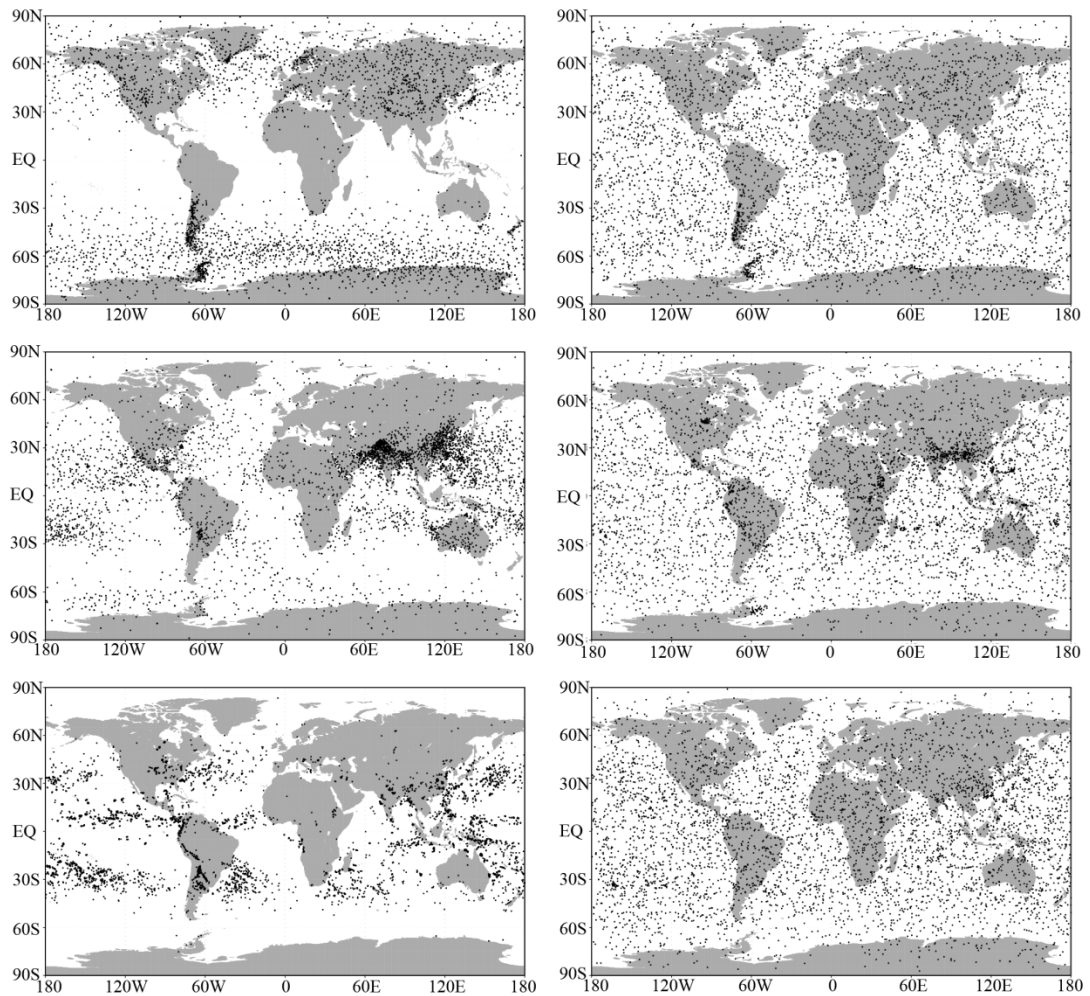
## **4. Statistical multiple regression experiment**

### **4.1 Temperature profile database**

A new database including a representative collection of 25,000 atmospheric profiles from the European Centre for Medium-range Weather Forecasts (ECMWF) was used for the statistical inversion experiments. The profiles were given in a 137-level vertical grid extending from the surface up to 0.01 hPa. The database was divided into five subsets focusing on diverse sampling characteristics such as temperature, specific humidity, ozone mixing ratio, cloud condensates, and precipitation. In contrast with earlier releases of the

ECMWF diverse profile database, the 137-level database places greater emphasis on preserving the statistical properties of sampled distributions produced by the Integrated Forecasting System (IFS) (Eresmaa and McNally, 2014; Brath et al., 2018). IFS-137 spans the period from September 1, 2013 to August 31, 2014. There are two operational analyses each day (at 00z and 12z), and approximately 13 000 atmospheric profiles over the ocean. The pressure levels adopted for IFS-137 are shown in Table A2 (see Table A2 in Appendix A).

The locations of selected profiles of temperature, specific humidity, and cloud condensate subsets of the IFS-91 and IFS-137 databases are plotted on the map in Fig. 7. In the IFS-91 database, the sampling is fully determined by the selection algorithm, which makes the geographical distributions very inhomogeneous. Selected profiles represent those regions where gradients of the sampled variable are the strongest: in the case of temperature, mid- and high-latitudes dominate, while humidity and cloud condensate subsets concentrate at low latitudes. However, the IFS-137 database shows a much more homogeneous spatial distribution in all the sampling subsets, which is a consequence of the randomized selection.



1880 **Figure 7.** Locations of selected profiles in the temperature (top),  
 1881 specific humidity (middle), and cloud condensate (bottom), sampled  
 1882 subsets of the IFS-91 (left) and IFS-137 (right) databases (from  
 1883 <https://www.nwpsaf.eu/site/update-137-level-nwp-profile-dataset/> ,  
 1884 2019).

1885

1886 The temporal distribution of the selected profiles is illustrated in Fig.

1887 8. The coverage of the IFS-137 data set is more homogeneous than

the IFS-91 data set. Moreover, the IFS-137 database supports the mode with input parameters, such as detection angle, 2 m temperature, and cloud information. Therefore, it is feasible to use the selected samples in a statistical multiple regression experiment.

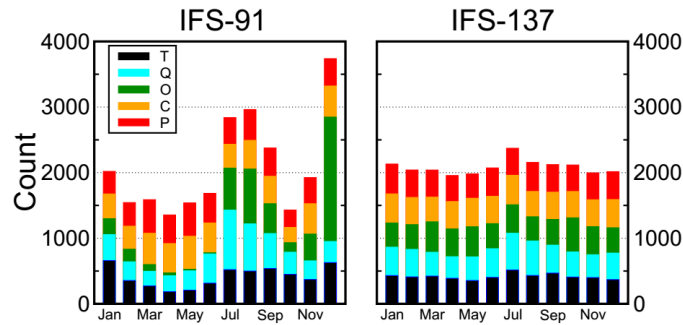


**Figure 8.** Distribution of profiles within the calendar months in IFS-91 (left) and IFS-137 (right) databases. Different subsets are shown in different colors. Black parts stand for temperature. Blue parts represent specific humidity. Green parts indicate ozone subset. Orange parts stand for cloud condensate. Red parts represent precipitation. The last access date is April 26th, 2019. (from <https://www.nwpsaf.eu/site/update-137-level-nwp-profile-dataset/>, 2019).

## 4.2 Experimental scheme

In order to verify the retrieval effectiveness of ICS, 5000 temperature profiles provided by the IFS-137 were used for statistical inversion comparison experiments. The steps are as follows:



(1) 5000 profiles and their corresponding surface factors, including surface air pressure, surface temperature, 2 m temperature, 2 m specific humidity, 10 m wind speed are put into the RTTOV mode. Then, the simulated AIRS spectra are obtained.

(2) The retrieval of temperature is carried out in accordance with Eq. (23). The 5000 profiles are divided into two groups. The first group of 2500 profiles is used to obtain the regression coefficient, and the second group of 2500 is used to test the result.

(3) Verification of the results. The test is carried out based on the standard deviation between the retrieval value and the true value.

### **4.3 Results and Discussion**

For the statistical inversion comparison experiments, the standard deviation of temperature retrieval is shown in Fig. 9. First, because PCS does not take channel sensitivity as a function of height into consideration, the retrieval result of PCS is inferior to that of ICS. Second, by comparing the results of ICS and NCS we found that below 100 hPa, since the method used in this paper considers near ground to be less of an influencing factor, the channel combination of ICS is slightly inferior to that of NCS, but the difference is small.

From 100 hPa to 10 hPa, the retrieval temperature of ICS in this paper is consistent with that of NCS, slightly better than the channel

selected for NCS. From 10 hPa to 0.02 hPa, near the space layer, the retrieval temperature of ICS is better than that of NCS. In terms of the standard deviation, the channel combination of ICS is slightly better than that of PCS from 100 hPa to 10 hPa. From 10 hPa to 0.02 hPa, the standard deviation of ICS is lower than that of NCS at about 1 K, meaning that the retrieval result of ICS is better than that of NCS.

In order to further illustrate the effectiveness of ICS, the mean improvement value of the ICS and its percentages compared with the PCS and NCS at different heights are shown in Table 1. Because PCS does not take channel sensitivity as a function of height into consideration, the retrieval result of PCS is inferior to that of ICS. In general, the accuracy of the retrieval temperature of ICS is improved. Especially, from 100 hPa to 0.01 hPa, the mean value of ICS is evidently improved by more than 0.5 K which means the accuracy can be improved by more than 11%. By comparing the results of ICS and NCS we found that below 100 hPa, since the method used in this paper considers near ground to be less of an influencing factor, the channel combination of ICS is slightly inferior to that of NCS, but the difference is small. From 100 hPa to 0.01 hPa, the mean value of ICS is improved by more than 0.36 K which means the accuracy can be improved by more than 9.6%.

**Table 1.** The mean improvement value of the ICS and its percentages compared with the PCS and NCS at different heights.

Pressure	Improved mean value /Percentage compared with PCS	Improved value /Percentage compared with NCS
hPa	K/%	K/%
surface-100hPa	0.24/10.77%	-0.04/-3.27%
100hPa-10hPa	0.15/5.08%	0.06/2.4%
10hPa-1hPa	0.04/0.64%	0.17/2.99%
1hPa-0.01hPa	0.52/11.92%	0.36/9.57%

This is because, as shown in Fig. 4: (1) Stratosphere and mesosphere is less affected by the ground surface, so the retrieval result of PCS is better than that of NCS. (2) Due to the method selected in this paper, there are more channels at 4.2  $\mu\text{m}$  for  $\text{N}_2\text{O}$  and 4.3  $\mu\text{m}$  for  $\text{CO}_2$  absorption bands, and the channel combination of PCS is superior to that of NCS for atmospheric temperature observation in the high temperature zone. Moreover, ICS takes channel sensitivity as a function of height into consideration, so its retrieval result is improved.

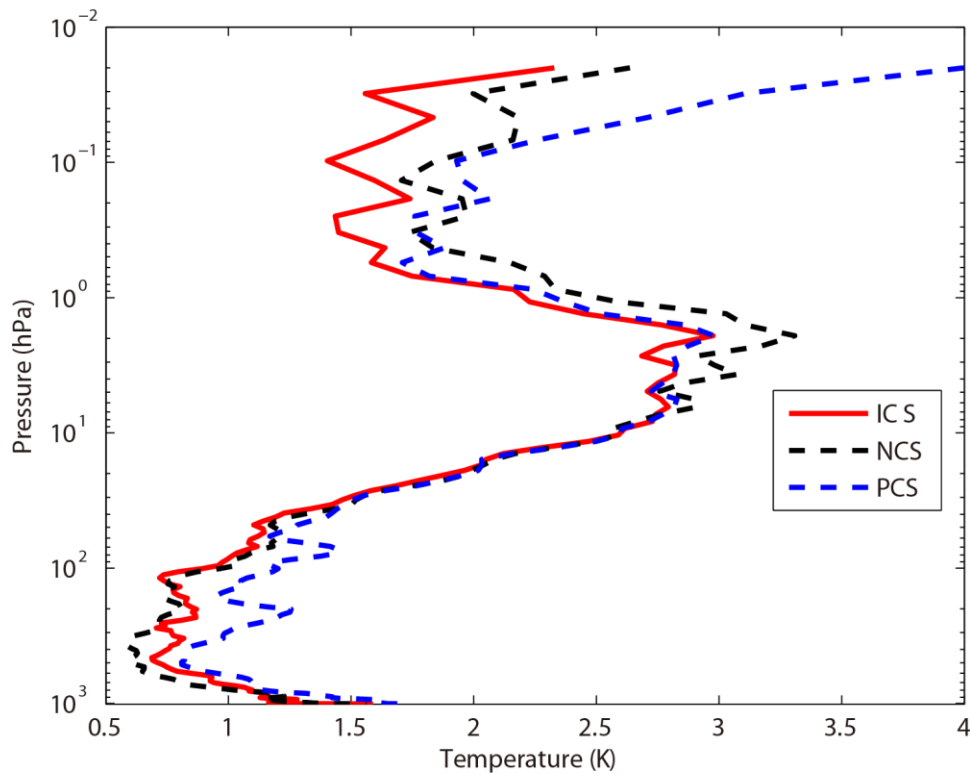


**Figure 9.** The temperature profile standard deviation of statistical inversion comparison experiments. Red line indicates the result of ICS. Black dotted line stands for the result of NCS. Blue dotted line represents the result of PCS.

## 5 Statistical inversion comparison experiments in four typical regions

The accuracy of the retrieval temperature varies from place to place and changes with atmospheric conditions. Therefore, in order to further compare the inversion accuracy under different atmospheric conditions, this paper has divided the atmospheric profile from the IFS-137 database introduced in Sect. 4 into four regions: equatorial

zone, subtropical region, mid-latitude region and Arctic. The average temperature profiles in these four regions are shown in Fig. 10. The retrieval temperature varies from place to place and changes with atmospheric conditions. In order to further compare the regional differences of inversion accuracy, the temperature standard deviations of ICS in four typical regions are compared in Sect. 5.2.

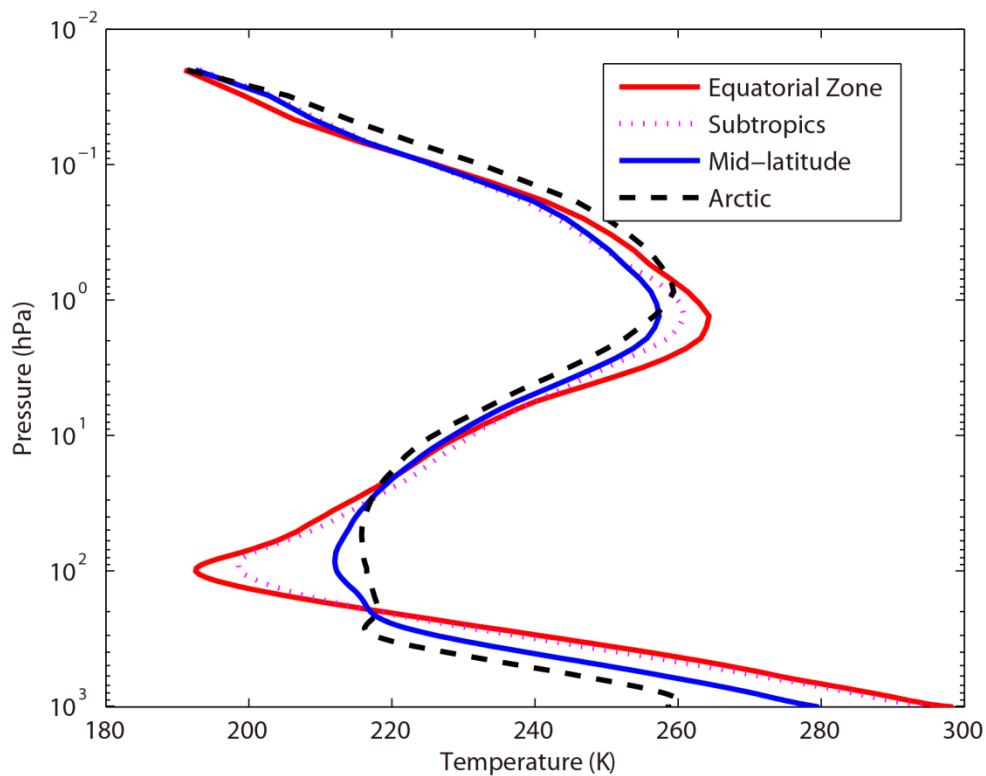


**Figure 10.** The average temperature profiles in four typical regions. Red line indicates the equatorial zone. Pink dotted line stands for the subtropics. Blue dotted line represents the mid-latitude region. Black dotted line stands for the Arctic.

1990

## 1991 **5.1 Experimental scheme**

1992 In order to further illustrate the different accuracy of the retrieval  
1993 temperature using our improved channel selection method under  
1994 different atmospheric conditions, the profiles in four typical regions  
1995 were used for statistical inversion comparison experiments. The  
1996 experimental steps are as follows:

1997 (1) 2500 profiles in Sect. 4 are used to work out the regression  
1998 coefficient.

1999 (2) The atmospheric profiles of the four typical regions: equatorial  
2000 zone, subtropical region, mid-latitude region and Arctic are used for  
2001 statistical inversion comparison experiments and test the result.(3)  
2002 Verification of the results. The test is carried out based on the  
2003 standard deviation between the retrieval value and the true value.

2004

## 2005 **5.2 Results and Discussion**

2006 Using statistical inversion comparison experiments in four typical  
2007 regions, the standard deviation of temperature retrieval is shown in  
2008 Fig. 11. Generally, the retrieval temperature by ICS is better than  
2009 that of NCS and PCS. In particular, above 1 hPa (the stratosphere  
2010 and mesosphere), the standard deviation of atmospheric temperature  
2011 can be improved by 1 K with PCS and NCS. Thus, ICS shows a

great improvement. The results were consistent with Sect. 4.

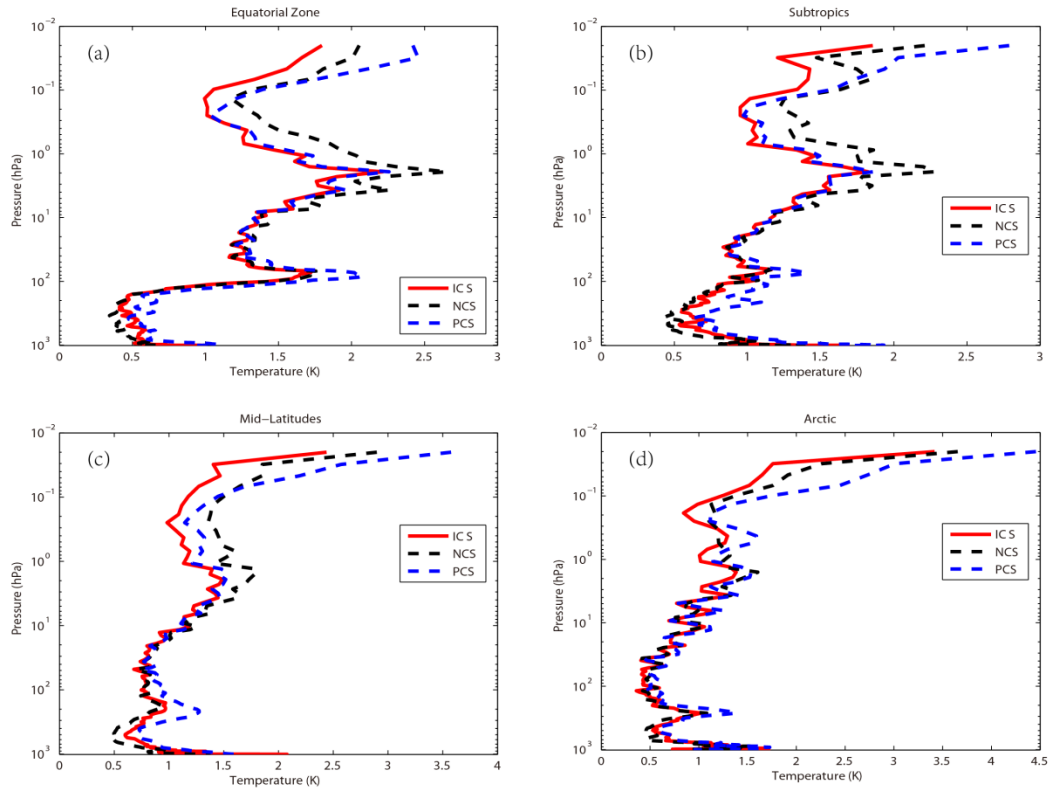


**Figure 11.** The temperature profile standard deviation of statistical inversion comparison experiments in four typical regions. Red line indicates the result of ICS. Black dotted line stands for the result of NCS. Blue dotted line represents the result of PCS. (a) Equatorial zone. (b) Subtropics. (c) Mid-latitudes. (d) Arctic.

In order to further compare the regional differences of inversion accuracy, the temperature standard deviation of ICS in four typical regions are compared in Fig. 12.

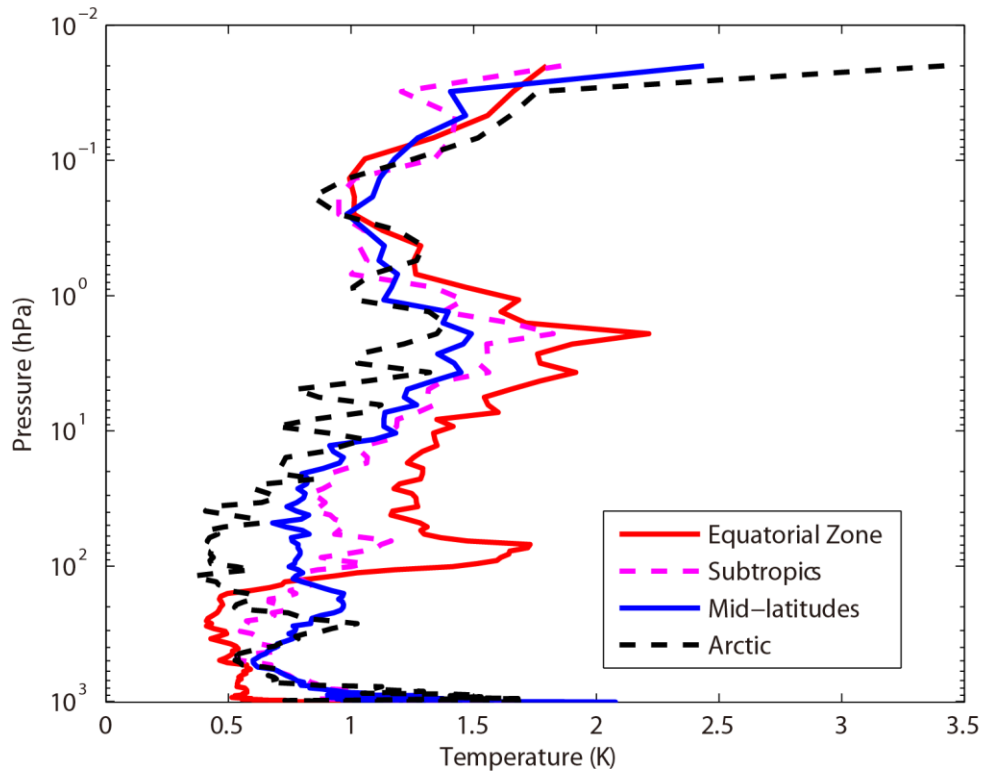


**Figure 12.** The temperature standard deviation of ICS in four typical regions. Red line indicates the result of equatorial zone. Pink dotted line represents the result of Subtropics. Blue line represents the result of Mid-latitudes. Black dotted line stands for the result of Arctic.

The temperature standard deviations of the ICS in the four typical regions are large (Fig. 12). Below 100 hPa, due to the high temperature in the equatorial zone, the channel combination of ICS is better than that of PCS and NCS for atmospheric temperature observation at higher temperature. The standard deviation is 0.5K. Due to the method selected in this paper there are more channels at



4.2  $\mu\text{m}$  for  $\text{N}_2\text{O}$  and 4.3  $\mu\text{m}$  for  $\text{CO}_2$  absorption bands which has been previously described in Sect. 3. Near the tropopause, the standard deviation of the equatorial zone increases sharply. It is also due to the sharp drops in temperature. However, the standard deviation of the Arctic is still around 0.5K. From 100hPa to 1hPa, the standard deviation of ICS is 0.5 K to 2K. With the increase of latitude, the effectiveness considerably increases. According to Fig. 11, ICS takes channel sensitivity as a function of height into consideration, so its retrieval result is better.

Although the improvements of ICS in the four typical regions are different, in general, the accuracy of the retrieval temperature of ICS is improved. Because PCS does not take channel sensitivity as a function of height into consideration, the retrieval result of PCS is inferior to that of ICS. In general, the accuracy of the retrieval temperature of ICS is improved.

## **7 Conclusions**

In recent years, the atmospheric layer in the altitude range of about 20–100 km has been named “the near space layer” by aeronautical and astronautical communities. It is between the space-based satellite platform and the aerospace vehicle platform, which is the transition zone between aviation and aerospace. Its unique resource

has attracted a lot of attention from many countries. Research and exploration, therefore, on and of the near space layer are of great importance. A new channel selection scheme and method for hyperspectral atmospheric infrared sounder AIRS data based on layering is proposed. The retrieval results of ICS concerning the near space atmosphere are particularly good. Thus, ICS aims to provide a new and an effective channel selection method for the study of the near space atmosphere using the hyperspectral atmospheric infrared sounder.

An improved channel selection method is proposed, based on information content in this paper. A robust channel selection scheme and method are proposed, and a series of channel selection comparison experiments are conducted. The results are as follows:

(1) Since ICS takes channel sensitivity as a function of height into consideration, the ARI of PCS only tends to be 0.38 and is not convergent. However, as the 100<sup>th</sup> iteration is approached, the ARI of ICS tends to be stable, reaching 0.54, while the distribution of the temperature weighting function is more continuous and closer to that of the actual atmosphere. Thus, in terms of the ARI, convergence, and the distribution of the temperature weighting function, ICS is better than PCS.

(2) Statistical inversion comparison experiments show that the

retrieval temperature of ICS in this paper is consistent with that of NCS. In particular, from 10 hPa to 0.02 hPa (the stratosphere and mesosphere), the retrieval temperature of ICS is obviously better than that of NCS at about 1 K. In general, the accuracy of the retrieval temperature of ICS is improved. Especially, from 100 hPa to 0.01 hPa, the accuracy of ICS can be improved by more than 11%. The reason is that stratosphere and mesosphere are less affected by the ground surface, so the retrieval result of ICS is better than that of NCS. Additionally, due to the method selected in this paper there are more channels at 4.2  $\mu\text{m}$  for the  $\text{N}_2\text{O}$  and at 4.3  $\mu\text{m}$  for the  $\text{CO}_2$  absorption bands; the channel combination of ICS is better than that of NCS for atmospheric temperature observation at higher temperature.

(3) Statistical inversion comparison experiments in four typical regions indicate that ICS in this paper is significantly better than NCS and PCS in different regions and shows latitudinal variations, which shows potential for future applications.

*Data availability.* The data used in this paper are available from the corresponding author upon request.

*Appendices*

## Appendix A

**Table A1.** Pressure levels adopted for RTTOV v12 54 pressure level coefficients and profile limits within which the transmittance calculations are valid. Note that the gas units here are ppmv. (From <https://www.nwpsaf.eu/site/software/rttov/>, RTTOV Users guide, 2019).

Level	Pressure	Tmax	Tmin	Qmax	Qmin	Q <sub>2</sub> max	Q <sub>2</sub> min	Q <sub>2</sub> Ref
Number	hPa	K	K	ppmv*	ppmv*	ppmv*	ppmv*	ppmv*
1	0.01	245.95	143.66	5.24	0.91	1.404	0.014	0.296
2	0.01	252.13	154.19	6.03	1.08	1.410	0.069	0.321
3	0.03	263.71	168.42	7.42	1.35	1.496	0.108	0.361
4	0.03	280.12	180.18	8.10	1.58	1.670	0.171	0.527
5	0.13	299.05	194.48	8.44	1.80	2.064	0.228	0.769
6	0.23	318.64	206.21	8.59	1.99	2.365	0.355	1.074
7	0.41	336.24	205.66	8.58	2.49	2.718	0.553	1.471
8	0.67	342.08	197.17	8.34	3.01	3.565	0.731	1.991
9	1.08	340.84	189.50	8.07	3.30	5.333	0.716	2.787
10	1.67	334.68	179.27	7.89	3.20	7.314	0.643	3.756
11	2.50	322.5	176.27	7.75	2.92	9.191	0.504	4.864
12	3.65	312.51	175.04	7.69	2.83	10.447	0.745	5.953
13	5.19	303.89	173.07	7.58	2.70	12.336	1.586	6.763
14	7.22	295.48	168.38	7.53	2.54	12.936	1.879	7.109
15	9.84	293.33	166.30	7.36	2.46	12.744	1.322	7.060
16	13.17	287.05	163.47	7.20	2.42	11.960	0.719	6.574
17	17.33	283.36	161.49	6.96	2.20	11.105	0.428	5.687
18	22.46	280.93	161.47	6.75	1.71	9.796	0.278	4.705
19	28.69	282.67	162.09	6.46	1.52	8.736	0.164	3.870
20	36.17	279.93	162.49	6.14	1.31	7.374	0.107	3.111

21	45.04	27315	164.66	5.90	1.36	6.799	0.055	2.478
22	55.44	265.93	166.19	6.21	1.30	5.710	0.048	1.907
23	67.51	264.7	167.42	9.17	1.16	4.786	0.043	1.440
24	81.37	261.95	159.98	17.89	0.36	4.390	0.038	1.020
25	97.15	262.43	163.95	20.30	0.01	3.619	0.016	0.733
26	114.94	259.57	168.59	33.56	0.01	2.977	0.016	0.604
27	134.83	259.26	169.71	102.24	0.01	2.665	0.016	0.489
28	156.88	260.13	169.42	285.00	0.01	2.351	0.013	0.388
29	181.14	262.27	17063	714.60	0.01	1.973	0.010	0.284
30	207.61	264.45	174.11	1464.00	0.01	1.481	0.013	0.196
31	236.28	270.09	177.12	2475.60	0.01	1.075	0.016	0.145
32	267.10	277.93	181.98	4381.20	0.01	0.774	0.015	0.110
33	300.00	285.18	184.76	6631.20	0.01	0.628	0.015	0.086
34	334.86	293.68	187.69	9450.00	1.29	0.550	0.016	0.073
35	371.55	300.12	190.34	12432.00	1.52	0.447	0.015	0.063
36	409.89	302.63	194.40	15468.00	2.12	0.361	0.015	0.057
37	449.67	304.43	198.46	18564.00	2.36	0.284	0.015	0.054
38	490.85	307.2	201.53	21684.00	2.91	0.247	0.015	0.052
39	532.56	31217	202.74	24696.00	3.67	0.199	0.015	0.050
40	572.15	31556	201.61	27480.00	3.81	0.191	0.012	0.050
41	618.07	318.26	189.95	30288.00	6.82	0.171	0.010	0.049
42	661.00	321.71	189.95	32796.00	6.07	0.128	0.009	0.048
43	703.59	327.95	189.95	55328.00	6.73	0.124	0.009	0.047
44	745.48	333.77	189.95	37692.00	8.71	0.117	0.009	0.046
45	786.33	336.46	189.95	39984.00	8.26	0.115	0.008	0.045
46	825.75	338.54	189.95	42192.00	7.87	0.113	0.008	0.043
47	863.40	342.55	189.95	44220.00	7.53	0.111	0.007	0.041
48	898.93	346.23	189.95	46272.00	7.23	0.108	0.006	0.040
49	931.99	34924	189.95	47736.00	6.97	0.102	0.006	0.038
50	962.26	349.92	189.95	51264.00	6.75	0.099	0.006	0.034

51	989.45	350.09	189.95	49716.00	6.57	0.099	0.006	0.030
52	1013.29	360.09	189.95	47208.00	6.41	0.094	0.006	0.028
53	1033.54	350.09	189.95	47806.00	6.29	0.094	0.006	0.027
54	1050.00	350.09	189.95	47640.00	6.19	0.094	0.006	0.027

2110

2111 **Table A2.** Pressure levels adopted for IFS-137 137 pressure levels

2112 (in hPa).

Level number	pressure hPa	Level number	pressure hPa	Level number	pressure hPa	Level number	pressure hPa	Level number	pressure hPa
1	0.02	31	12.8561	61	106.4153	91	424.019	121	934.7666
2	0.031	32	14.2377	62	112.0681	92	441.5395	122	943.1399
3	0.0467	33	15.7162	63	117.9714	93	459.6321	123	950.9082
4	0.0683	34	17.2945	64	124.1337	94	478.3096	124	958.1037
5	0.0975	35	18.9752	65	130.5637	95	497.5845	125	964.7584
6	0.1361	36	20.761	66	137.2703	96	517.4198	126	970.9046
7	0.1861	37	22.6543	67	144.2624	97	537.7195	127	976.5737
8	0.2499	38	24.6577	68	151.5493	98	558.343	128	981.7968
9	0.3299	39	26.7735	69	159.1403	99	579.1926	129	986.6036
10	0.4288	40	29.0039	70	167.045	100	600.1668	130	991.023
11	0.5496	41	31.3512	71	175.2731	101	621.1624	131	995.0824
12	0.6952	42	33.8174	72	183.8344	102	642.0764	132	998.8081
13	0.869	43	36.4047	73	192.7389	103	662.8084	133	1002.225
14	1.0742	44	39.1149	74	201.9969	104	683.262	134	1005.356
15	1.3143	45	41.9493	75	211.6186	105	703.3467	135	1008.224
16	1.5928	46	44.9082	76	221.6146	106	722.9795	136	1010.849
17	1.9134	47	47.9915	77	231.9954	107	742.0855	137	1013.25
18	2.2797	48	51.199	78	242.7719	108	760.5996		
19	2.6954	49	54.5299	79	253.9549	109	778.4661		
20	3.1642	50	57.9834	80	265.5556	110	795.6396		
21	3.6898	51	61.5607	81	277.5852	111	812.0847		
22	4.2759	52	65.2695	82	290.0548	112	827.7756		
23	4.9262	53	69.1187	83	302.9762	113	842.6959		
24	5.6441	54	73.1187	84	316.3607	114	856.8376		
25	6.4334	55	77.281	85	330.2202	115	870.2004		
26	7.2974	56	81.6182	86	344.5663	116	882.791		
27	8.2397	57	86.145	87	359.4111	117	894.6222		
28	9.2634	58	90.8774	88	374.7666	118	905.7116		
29	10.372	59	95.828	89	390.645	119	916.0815		

*Author contributions.* ZS contributed the central idea. SC, ZS and HD conceived the method, developed the retrieval algorithm and discussed the results. SC analyzed the data, prepared the figures and wrote the paper. WG contributed to refining the ideas, carrying out additional analyses. All co-authors reviewed the paper.

*Competing interests.* The authors declare that they have no conflict of interest.

*Acknowledgements.* The study was supported by the National Key Research Program of China: Development of high-resolution data assimilation technology and atmospheric reanalysis data set in East Asia (Research on remote sensing telemetry data assimilation technology, Grant no. 2017YFC1501802). The study was also supported by the National Natural Science Foundation of China (Grant no. 41875045) and Hunan Provincial Innovation Foundation for Postgraduate (Grant no. CX2018B033 and no. CX2018B034).

## References

Aires, F., Schmitt, M., Chedin, A., and Scott, N.: The “weighting smoothing” regularization of MLP for Jacobian stabilization,

2134 IEEE. T. Neural. Networks., 10, 1502-1510,  
 2135 <https://doi.org/10.1109/72.809096>, 1999.

2136 Aires, F., Chédin, Alain., Scott, N. A., and Rossow, W. B.: A  
 2137 regularized neural net approach for retrieval of atmospheric and  
 2138 surface temperatures with the IASI instrument, J. Appl. Meteorol.,  
 2139 41,144-159,  
 2140 [https://doi.org/10.1175/1520-0450\(2002\)041<0144:ARNNAF>2.0](https://doi.org/10.1175/1520-0450(2002)041<0144:ARNNAF>2.0)  
 2141 .CO;2, 2002.

2142 Aumann, H. H.: Atmospheric infrared sounder on the earth  
 2143 observing system, Optl. Engr., 33, 776-784,  
 2144 <https://doi.org/10.1117/12.159325>, 1994.

2145 Aumann, H. H., Chahine, M. T., Gautier, C., and Goldberg, M.:  
 2146 AIRS/AMSU/HSB on the Aqua mission: design, science objective,  
 2147 data products, and processing systems, IEEE. Trans. GRS.,  
 2148 41,253-264, <http://dx.doi.org/10.1109/TGRS.2002.808356>, 2003.

2149 Brath, M., Fox, S., Eriksson, P., Harlow, R. C., Burgdorf, M., and  
 2150 Buehler, S. A.: Retrieval of an ice water path over the ocean from  
 2151 ISMAR and MARSS millimeter and submillimeter brightness  
 2152 temperatures, Atmos. Meas. Tech., 11, 611–632,  
 2153 <https://doi.org/10.5194/amt-11-611-2018>, 2018.

2154 Chahine, M. I.: A general relaxation method for inverse solution of  
 2155 the full radiative transfer equation, J. Atmos. Sci., 29, 741-747,



2156 [https://doi.org/10.1175/1520-0469\(1972\)029<0741:AGRMFI>2.0](https://doi.org/10.1175/1520-0469(1972)029<0741:AGRMFI>2.0).  
 2157 CO;2, 1972.

2158 Chang, K. W, L'Ecuyer, T. S., Kahn, B. H., and Natraj, V.:  
 2159 Information content of visible and midinfrared radiances for  
 2160 retrieving tropical ice cloud properties, J. Geophys. Res., 122,  
 2161 <https://doi.org/10.1002/2016JD026357>, 2017.

2162 Chedin, A., Scott, N. A., Wahiche, C., and Moulinier, P.: The  
 2163 improved initialization inversion method: a high resolution  
 2164 physical method for temperature retrievals from satellites of the  
 2165 tiros-n series, J. Appl. Meteor., 24, 128-143,  
 2166 [https://doi.org/10.1175/1520-0450\(1985\)024<0128:TIHIMA>2.0.C](https://doi.org/10.1175/1520-0450(1985)024<0128:TIHIMA>2.0.C)  
 2167 O;2, 1985.

2168 Cyril, C., Alain, C., and Scott, N. A.: Airs channel selection for CO<sub>2</sub>  
 2169 and other trace-gas retrievals, Q. J. Roy. Meteor. Soc., 129,  
 2170 2719-2740, <https://doi.org/10.1256/qj.02.180>, 2003.

2171 Du, H. D., Huang, S. X., and Shi, H. Q.: Method and experiment of  
 2172 channel selection for high spectral resolution data, Acta. Physica.  
 2173 Sinica., 57, 7685-7692, 2008 .

2174 Dudhia, A., Jay, V. L., and Rodgers, C. D.: Microwindow selection  
 2175 for high-spectral-resolution sounders, Appl. Opt. 41, 3665-3673,  
 2176 <https://doi.org/10.1364/AO.41.003665>, 2002.

2177 Eresmaa, R. and McNally, A. P.: Diverse profile datasets from the

2178 ECMWF 137-level short-range forecasts, Tech. rep., ECMWF,  
 2179 2014.

2180 Eyre, J. R., Andersson E., and McNally, A. P.: Direct use of  
 2181 satellite sounding radiances in numerical weather prediction, High  
 2182 Spectral Resolution Infrared Remote Sensing for Earth's Weather  
 2183 and Climate Studies, Springer, Berlin, Heidelberg,  
 2184 [https://doi.org/10.1007/978-3-642-84599-4\\_25](https://doi.org/10.1007/978-3-642-84599-4_25), 1993.

2185 Fang, Z. Y.: The evolution of meteorological satellites and the  
 2186 insight from it, Adv. Meteorol. Sci. Technol., 4, 27-34,  
 2187 <https://doi.org/10.3969/j.issn.2095-1973.2014.06.003>, 2014.

2188 Gong, J., Wu, D. L., and Eckermann, S. D.: Gravity wave variances  
 2189 and propagation derived from AIRS radiances, Atmos. Chem.  
 2190 Phys., 11, 11691-11738,  
 2191 <https://doi.org/10.5194/acp-12-1701-2012>, 2011.

2192 He, M. Y., Du, H. D., Long, Z. Y., and Huang, S. X.: Selection of  
 2193 regularization parameters using an atmospheric retrievable index  
 2194 in a retrieval of atmospheric profile, Acta. Physica Sinica., 61,  
 2195 024205-160, 2012.

2196 Hoffmann, L. and Alexander, M. J.: Retrieval of stratospheric  
 2197 temperatures from atmospheric infrared sounder radiance  
 2198 measurements for gravity wave studies, J. Geophys. Res. Atm.,  
 2199 114, <https://doi.org/10.1029/2008JD011241>, 2009.

2200 Huang, H. L., Li, J., Baggett, K., Smith, W. L., and Guan, L.:  
 2201 Evaluation of cloud-cleared radiances for numerical weather  
 2202 prediction and cloud-contaminated sounding applications,  
 2203 Atmospheric and Environmental Remote Sensing Data Processing  
 2204 and Utilization: Numerical Atmospheric Prediction and  
 2205 Environmental Monitoring, I. S. O. Photonics.,  
 2206 <https://doi.org/10.1117/12.613027>, 2005.

2207 Kuai, L., Natraj, V., Shia, R. L., Miller, C., and Yung, Y. L.: Channel  
 2208 selection using information content analysis: a case study of CO<sub>2</sub>  
 2209 retrieval from near infrared measurements. J. Q. S. Radiative.  
 2210 Transfer., 111, 1296-1304,  
 2211 <https://doi.org/10.1016/j.jqsrt.2010.02.011>, 2010.

2212 Li, J., Wolf, W. W., Menzel, W. P., Paul, Menzel. W., Zhang, W. J.,  
 2213 Huang, H. L., and Achtor, T. H.: Global soundings of the  
 2214 atmosphere from ATOVS measurements: the algorithm and  
 2215 validation, J. Appl. Meteor., 39, 1248-1268,  
 2216 [https://doi.org/10.1175/1520-0450\(2000\)039<1248:GSOTAF>2.0.](https://doi.org/10.1175/1520-0450(2000)039<1248:GSOTAF>2.0.CO;2)  
 2217 CO<sub>2</sub>, 2000.

2218 Li, J., Liu, C. Y., Huang, H. L., Schmit, T. J., Wu, X., Menzel, W. P.,  
 2219 and Gurka, J. J.: Optimal cloud-clearing for AIRS radiances using  
 2220 MODIS, IEEE. Trans. GRS. , 43, 1266-1278, [http://dx.doi.org/](http://dx.doi.org/10.1109/tgrs.2005.847795)  
 2221 [10.1109/tgrs.2005.847795](http://dx.doi.org/10.1109/tgrs.2005.847795), 2005.

2222 Liu, Z. Q.: A regional ATOVS radiance-bias correction scheme for  
 2223 radiance assimilation, *Acta. Meteorologica. Sinica.*, 65, 113-123,  
 2224 2007.

2225 Lupu, C., Gauthier, P., and Laroche, Stéphane.: Assessment of the  
 2226 impact of observations on analyses derived from observing system  
 2227 experiments, *Mon. Weather. Rev.*, 140, 245-257,  
 2228 <https://doi.org/10.1175/MWR-D-10-05010.1>, 2012.

2229 Menke, W.: *Geophysical Data Analysis: Discrete Inverse Theory*,  
 2230 Acad. Press., Columbia University, New York,  
 2231 <https://doi.org/10.1016/B978-0-12-397160-9.00019-9>, 1984.

2232 Menzel, W. P., Schmit, T. J., Zhang, P. and Li, J.: Satellite-based  
 2233 atmospheric infrared sounder development and applications, *Bull.*  
 2234 *Amer. Meteor. Soc.*, 99, 583–603,  
 2235 <https://doi.org/10.1175/BAMS-D-16-0293.1>, 2018.

2236 Prunet, P., Thépaut J. N., and Cass, V.: The information content of  
 2237 clear sky IASI radiances and their potential for numerical weather  
 2238 prediction, *Q. J. Roy. Meteor. Soc.*, 124, 211-241,  
 2239 <https://doi.org/10.1002/qj.49712454510>, 2010.

2240 Xu, Q.: Measuring information content from observations for data  
 2241 assimilation: relative entropy versus shannon entropy difference,  
 2242 *Tellus. A.*, 59, 198-209,  
 2243 <https://doi.org/10.1111/j.1600-0870.2006.00222.x>, 2007.

2244 Rabier, F., Fourrié, N., and Chafai, D.: Channel selection methods  
 2245 for infrared atmospheric sounding interferometer radiances, Q. J.  
 2246 Roy. Meteor. Soc., 128, 1011-1027,  
 2247 <https://doi.org/10.1256/0035900021643638>, 2010.

2248 Richardson, M. and Stephens, G. L.: Information content of oco-2  
 2249 oxygen a-band channels for retrieving marine liquid cloud  
 2250 properties, Atmospheric Measurement Techniques, 11, 1-19,  
 2251 <https://doi.org/10.5194/amt-11-1515-2018>, 2018.

2252 Rodgers, C. D.: Information content and optimisation of high  
 2253 spectral resolution remote measurements, Adv. Spa. Research, 21,  
 2254 136-147, [https://doi.org/10.1016/S0273-1177\(97\)00915-0](https://doi.org/10.1016/S0273-1177(97)00915-0), 1996.

2255 Rodgers, C. D.: Inverse Methods for Atmospheric Sounding, Inverse  
 2256 methods for atmospheric sounding, World Scientific,  
 2257 <https://doi.org/10.1142/3171>, 2000.

2258 Saunders, R., Hocking, J., Turner, E., Rayer, P., Rundle, D., Brunel,  
 2259 P., Vidot, J., Roquet, P., Matricardi, M., Geer, A., Bormann, N.,  
 2260 and Lupu, C.: An update on the RTTOV fast radiative transfer  
 2261 model (currently at version 12), Geosci. Model Dev., 11,  
 2262 2717-2737, <https://doi.org/10.5194/gmd-11-2717-2018>, 2018.

2263 Susskind, J., Barnett, C. D. and Blaisdell, J. M.: Retrieval of  
 2264 atmospheric and surface parameters from AIRS/AMSU/HSB data  
 2265 in the presence of clouds, IEEE Trans. Geosci. Remote Sensing,

41, 390-409, <https://doi.org/10.1109/TGRS.2002.808236>, 2003.

Smith, W. L., Woolf, H. M., and Revercomb, H. E.: Linear simultaneous solution for temperature and absorbing constituent profiles from radiance spectra, *Appl. Optics.*, 30, 1117, <https://doi.org/10.1364/AO.30.001117>, 1991.

Wakita, H., Tokura, Y., Furukawa, F., and Takigawa, M.: Study of the information content contained in remote sensing data of atmosphere, *Acta. Physica. Sinica.*, 59, 683-691, 2010.

Wang, G., Lu, Q. F., Zhang, J. W., and Wang, H. Y.,.: Study on method and experiment of hyper-spectral atmospheric infrared sounder channel selection, *Remote Sensing Technology and Application.*, 29, 795-802 , 2014.

Zhang, J. W., Wang, G., Zhang, H., Huang J., Chen J., and Wu, L. L.: Experiment on hyper-spectral atmospheric infrared sounder channel selection based on the cumulative effect coefficient of principal component, *Journal of Nanjing Institute of meteorology*, 1, 36-42, <http://dx.doi.org/10.3969/j.issn.1674-7097.2011.01.005>, 2011.